IWLR 18-7.65 Rev 1

Sequential Processing of ILRS Observations – Experiences over the last 5 years

David A. Vallado[*], James Woodburn[†], Tom Johnson[‡]

Satellite Laser Ranging (SLR) is an extremely precise method of tracking satellites. This paper documents our experiences and estimated accuracies obtained in the last 5 years while processing SLR observations of satellites in support of the Commercial Space Operations Center (ComSpOC) internal calibration activities. Such precise Orbit Determination (OD) requires special algorithms and processes. To calibrate our internal sensors, we use an extended sequential filter, smoothing methods, and analytic partials employed by the Orbit Determination Tool Kit (ODTK) to obtain highly accurate ephemerides. ODTK also lets us form realistic error estimates generally not obtainable via batch least squares estimation techniques. We discuss the overall setup process, and the revised setup to update processing for the current ILRS configuration.

INTRODUCTION

Satellite Laser Ranging (SLR) is a satellite tracking method with measurement accuracy at about one centimeter or better. Such high accuracy makes SLR useful for many scientific purposes, particularly geodetic research. But because of its public availability, SLR has also found increasing application towards more common operational endeavors related to orbit determination. For example, available SLR observations can be leveraged during the development of precise orbit-determination software because of its high accuracy, and because good fits to the SLR tracking data provides a comparable measure of the accuracy of orbit determination modeling. With access to non-SLR tracking of an SLR satellite, SLR-derived orbits can also be used for tracking-sensor calibration. We followed this process for several years now at Analytical Graphics Inc. (AGI) as part of our calibration effort for the Commercial Space Operations Center (ComSpOC). Specifically, measurement residuals are computed relative to the SLR-derived orbits to reveal constant and time varying biases and characterize measurement noise. Using the latest sensor network configuration maximizes initial performance in operational analyses.

The Orbit Determination Toolkit (ODTK, Vallado et al. 2010) built by AGI approaches precision orbit determination using a specialized form of the Extended Kalman (sequential) Filter (EKF) in combination with either fixed-interval or variable lag smoothing. The filter-smoother approach is somewhat novel among existing orbit-determination packages that incorporate high-accuracy modeling. Specifically, the sequential processing approach requires the specification of parameters to characterize the time varying nature of variables generally considered to be constants or segmented constants during Batch Weighted Least Squares (BWLS) estimation and not otherwise characterized through the International Laser Ranging System (ILRS). A process is therefore required whereby these parameters must be established. Such parameters are reflected in the tracking-system objects supplied with ODTK. Although ODTK's SLR processing capabilities have been used in various applications since ODTK became commercially available over a decade ago, the results of ODTK's sequential approach to SLR had not been systematically compared to external products beyond the fit to the SLR observations. Vallado, Woodburn and Deleflie (2014) detailed the formation of Laser Geodynamics Satellite or Laser Geometric Environmental Observation Survey (LAGEOS) (1 and 2), Ajisai (the Japanese name for the Hydrangea plant, but also referred to as the Experimental Geodetic Satellite or Payload, EGS/EGP), Etalon (1 and 2), Laser Relativity Satellite (LARES), Larets, Satellite de Taille Adaptée avec Réflecteurs Laser pour les Etudes de la Terre (STARLETTE), and Stella ephemerides. These ephemerides were then compared with independent definitive orbits from UT Austin Center for Space Research (CSR), and ILRS Analysis Centers. Sequential processing results showed comparable accuracy to the published reference orbits.

Relevant features to account for in the setup of reference orbit generation are reviewed, and statements are made concerning our experience in processing several years' worth of SLR data.

[*] Senior Research Astrodynamicist, Center for Space Standards and Innovation, Analytical Graphics Inc., 7150 Campus Dr., Suite 260, Colorado Springs, Colorado, 80920-6522. dvallado@agi.com

[†] Chief Orbital Scientist, Analytical Graphics Inc., 220 Valley Creek Blvd, Exton PA 19341. jwoodburn@agi.com

[‡] Vice President, Engineering, Analytical Graphics Inc., 220 Valley Creek Blvd, Exton PA 19341. tjohnson@agi.com

ILRS NETWORK

The ILRS network consists of numerous stations distributed around the world, as shown in Fig. 1.

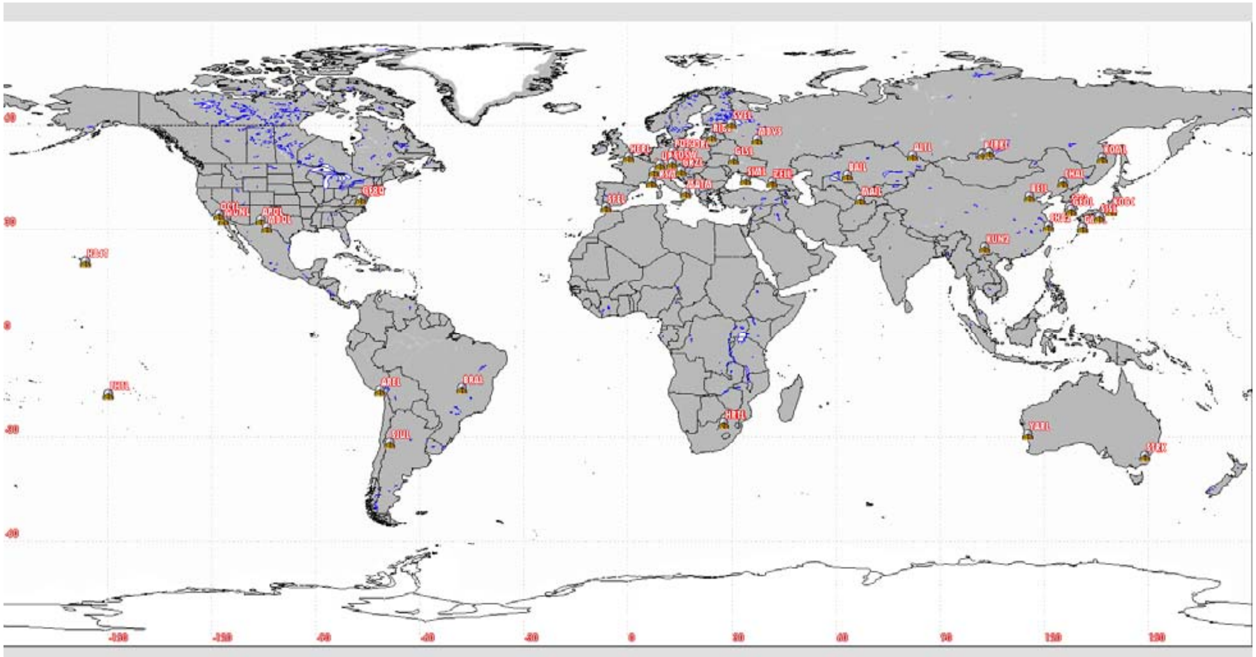

Figure 1: ILRS Station Locations: Approximate locations for the ILRS network are shown.

These stations change over time due to upgrades, closures, and new additions. Accurate analyses require that current information be used in the representations of these sites[*]. As of September 2018, the current list of ILRS stations is shown in Table 1.

Several steps are required to properly configure the ILRS network for processing within ODTK. Updates may be necessary for inter-year sensor changes depending on the length of the desired orbit fit. One must be careful to distinguish between the station locations and the precise location of the optical instruments. The precise positions are given as offsets (or *eccentricities*) in Earth Fixed Cartesian (XYZ) coordinates, from the given station positions[†]. These *eccentricities* are generally under about 15 m.

- Station nomenclature is necessary to properly identify each sensor. Note that the IERS DOME and CDDIS SOD numbers may be better for some applications. In cases where multiple designations exist for a single sensor, the CDDIS SOD number seems to be the most useful for distinguishing each.
- Cartesian position solutions consistent with SLRF-2014 are located on the Internet[‡]. The SLRF-2014 is related to the ITRF-2014, but it is rescaled to the SLR specific scale deduced from the SLR data. The Cartesian Earth Fixed (XYZ) coordinates are readily converted to geodetic latitude and longitude (Vallado 2013:172-173) if needed.
- Station eccentricities (XYZ) are added to the Cartesian coordinates to locate the sensor most precisely.

It is useful to perform a gross check of the site locations in Google Earth. Although Google Earth is not a precision geo-registration tool, it can help identify gross errors. For this set of stations, the Google Earth depiction independently confirmed that the locations provided in Table 1 are accurate.

Historical optical instrument locations are also available on the Internet for historical studies[§].

[*] https://ilrs.cddis.eosdis.nasa.gov/network/stations/index.html. The site lists active, engineering, inactive, and future stations. (accessed Sep 2018)

[†] ftp://cddis.gsfc.nasa.gov/slr/slrocc/ecc_xyz.snx. Note that the "xyz" coordinates are sometimes preferred because they add directly to the Cartesian sensor location. Values above about 15m are considered less reliable. These values should be added to the base coordinates to find a more precise sensor location. (accessed Sep 2018)

[‡] ftp://cddis.nasa.gov/slr/products/resource/SLRF2014_POS+VEL_2030.0_180504.snx. (Accessed Sep 2018)

[§] https://ilrs.cddis.eosdis.nasa.gov/network/stations/pre-ILRS_Stations/index.html. (Accessed Sep 2018)

Table 1: ILRS Station Locations: ILRS station locations are given as of September 2018. Precise locations are given in Earth fixed Cartesian (XYZ) coordinates. We list latitude longitude values here for the reader's convenience, but be aware that they result from geodetic Cartesian coordinates plus any sensor eccentricities. GRSM (7845) is now able to track both the Moon (LLR) and SLR satellites (MEO = SLR + LLR). The last 5 sensors below are engineering stations.

SLR Sensors

ID #	Location	Name	Type	Latitude	Longitude	Alt (m)	Open	Last Msg	Notes
1824	Golosiiv, Ukraine	GLSL	SLR	50.363132	30.495885	212.1	1-Apr-97	8-Jun-18	
1868	Komsomolsk-na-Amure, Russia	KOML	SLR	50.694603	136.743833	270.0	1-May-92	27-Jan-14	
1873	Simeiz, Ukraine	SIML	SLR	44.413188	33.990954	364.8	1-May-88	22-Mar-17	
1874	Mendeleevo 2, Russia	MDVS	SLR	56.027734	37.224904	227.7		14-Aug-13	
1879	Altay, Russia	ALTL	SLR	51.343900	82.177292	369.7	15-Sep-04	25-Mar-09	
1884	Riga, Latvia	RIGL	SLR	56.948553	24.059078	31.6	1-Sep-87	27-Jul-17	
1886	Arkhyz, Russia	ARKL	SLR	43.649842	41.431472	2077.9		15-Feb-12	
1887	Baikonur, Kazakhstan	BAIL	SLR	45.704969	63.342415	98.4		13-Feb-12	
1888	Svetloe, Russia	SVEL	SLR	60.533155	29.780455	69.5		31-Jan-12	
1889	Zelenchukskya, Russia	ZELL	SLR	43.788670	41.565383	1155.8		31-Jan-12	
1890	Badary, Russia	BADL	SLR	51.770034	102.235361	803.7		31-Jan-12	
1891	Irkutsk, Russia	IRKL	SLR	52.219139	104.316389	506.0		2-Sep-14	
1893	Katzively, Ukraine	KTZL	SLR	44.393174	33.970128	68.5	20-Sep-82	2-Aug-11	
7045	Apache Point, NM	APOL	SLR	32.780361	-105.820417	2788.0		29-Jun-09	from web, lat lon
7080	McDonald Observatory, TX	MDOL	SLR	30.680267	-104.015215	2004.7	1-Jan-88	9-Mar-17	
7090	Yarragadee, Australia	YARL	SLR	-29.046491	115.346723	241.7	1-Jul-79	13-Dec-18	
7105	Greenbelt, MD	GODL	SLR	39.020605	-76.827724	19.6	1-Mar-81	20-Mar-18	
7110	Monument Peak, CA	MONL	SLR	32.891740	-116.422705	1839.4	15-Aug-83	7-Jun-17	
7119	Haleakala, HI	HA4T	SLR	20.706491	-156.256947	3056.7	15-Sep-06	4-May-18	
7124	Tahiti, French Polynesia	THTL	SLR	-17.576803	-149.606240	94.8	1-Aug-97	31-Oct-12	
7237	Changchun, China	CHAL	SLR	43.790512	125.443462	274.6	1-Jan-83	10-Apr-18	
7249	Beijing, China	BEIL	SLR	39.606933	115.892059	82.2	12-Dec-88	3-Jan-12	
7308	Koganei, Japan(CRL)	KOGC	SLR	35.710085	139.489127	122.8	1-Mar-88	21-Oct-02	no tropo
7358	Tanegashima, Japan	GMSL	SLR	30.556508	131.015422	141.8	25-Mar-04	9-May-17	
7394	Sejong City, Rep of Korea	SEJL	SLR	36.520992	127.302912	173.7	10-Jul-05	6-Sep-18	
7395	Geochang, Republic of Korea	GEOL	SLR	35.590166	127.920065	934.5		25-Sep-18	from web
7403	Arequipa, Peru	AREL	SLR	-16.465718	-71.492982	2489.2	10-Jul-92	19-Jan-18	
7406	San Jaun, Argentina	SJUL	SLR	-31.508625	-68.623158	727.7	28-Nov-05	4-Apr-06	no tropo
7407	Brasilia, Brazil	BRAL	SLR	-15.773068	-47.865293	1029.3	17-Apr-02	26-Aug-14	after earthquake
7501	Hartebeesthoek, South Africa	HARL	SLR	-25.889707	27.686147	1407.2	12-Sep-93	5-Dec-18	
7503	Hartebeesthoek, South Africa	HRTL	SLR	-25.889209	27.686141	1412.7		4-Sep-18	
7810	Zimmerwald, Switzerland	ZIML	SLR	46.877231	7.465223	951.7	3-Jul-95	5-Mar-18	
7811	Borowiec, Poland	BORL	SLR	52.276982	17.074590	123.0	13-May-88	15-Jun-18	
7819	Kunming, China	KUN2	SLR	25.029791	102.797683	1987.7		8-Feb-18	
7821	Shanghai, China	SHA2	SLR	31.096094	121.186614	100.4	10-Jul-05	14-Nov-15	
7824	San Fernando, Spain	SFEL	SLR	36.465256	-6.205308	98.7	4-Apr-99	11-Jun-15	
7825	Mt Stromlo, Australia	STL3	SLR	-35.316141	149.009881	805.4	1-Aug-04	20-Jul-18	
7827	Wettzell, Germany	SOSW	SLR	49.144941	12.878101	663.6	1-Mar-89	11-May-17	
7838	Simosato, Japan	SISL	SLR	33.577693	135.937038	102.0	31-Jan-82	27-Mar-18	
7839	Graz, Austria	GRZL	SLR	47.067138	15.493365	539.8	1-Nov-81	26-Jun-18	
7840	Herstmonceux, United Kingdom	HERL	SLR	50.867383	0.336127	75.8	1-Jan-82	5-Feb-18	
7841	Potsdam, Germany	POT3	SLR	52.383013	13.061436	127.7	20-Jul-01	14-Nov-18	
7845	Grasse, France (MéO)	GRSM	SLR	43.754634	6.921575	1323.7	1-Sep-80	6-Mar-18	
7941	Matera, Italy (MLRO)	MATM	SLR	40.648672	16.704613	537.4	1-Jan-00	2-Sep-14	
8834	Wettzell, Germany (WLRS)	WETL	SLR	49.144419	12.878012	665.8	1-Mar-89	27-Jul-18	
7040	Wrightwood, California	OCTL	SLR	34.381764	-117.682811	2200.0		3-Feb-05	from web, lat lon
7125	Greenbelt, Maryland	GF8Q	SLR	39.020244	-76.827482	18.8		19-Oct-14	
7816	Stuttgart, Germany	UROL	SLR	48.782402	9.196433	400.8		20-Apr-18	from web
7826	Mt Stromlo, Australia	STRK	SLR	-35.316300	149.009800	806.6		10-Aug-04	from webITRF 2000
7865	Stafford, Virginia	STAL	SLR	38.499217	-77.371108	23.9		15-Nov-16	from web

In the time since our previous setup, there were several new sensors and sensors that were retired.

Table 2: Sensor Changes: Several sensors were added while several were retired. Some dates are included for the last messages from individual sensors.

New Sensors			Old Sensors		
STAL	7865		LVIL	1831	
OCTL	7040		MAIN	1863	
GF8Q	7125		MDVL	1870	
GEOL	7395		WUHL	7231	
HRTL	7503		KOGL	7328	
UROL	7816		DAEK	7359	Jun 15
KUN2	7819		CONL	7405	
STRK	7826		METL	7806	Nov 17
			KUNL	7820	Jun 14
			HLWL	7831	Jul 16
			RIYL	7832	

OBSERVATIONAL DATA

Historically, several formats have been used for laser ranging data. In the past, Full Rate (FR) and Normal Point (NPT) data were common. Recognizing the need for additional accuracy and expanded data, the ILRS has transitioned to the Consolidated Range Data (CRD NPT) format for most satellites. The CRD format was developed over the 2008-2010 timeframe and became official on April 9, 2012. Some archived data from 2010 may differ from current formats as the sites didn't all implement the precise format at the same time. While the older FR and NPT formats are no longer supported*, the .npt file extension is still used, but the header contains the CRD nomenclature. ODTK reads both forms properly.

ORBIT DETERMINATION

ODTK is a commercial software product from AGI that performs orbit determination and analysis. Its key features include a tracking-data simulator, a sequential (specialized form of the EKF) filter, a fixed-interval smoother and a variable lag smoother. The filter runs forward in time and is used to obtain current and predicted estimates of the orbit and associated parameters. The fixed-interval smoother runs backwards in time, starting with the end state of the filter, to generate definitive post-fit estimates. The variable-lag smoother serves the same function as the fixed-interval smoother but is executed concurrently with the filter process. A variety of tools are available to aid the researcher and analyst, including estimation of multiple satellite parameters and time-varying measurement biases, autonomous measurement editing, and data reporting and graphing.

Of specific interest to the current research, the methodology used for parameter estimation (i.e., the unknowns associated with the force model and sensor system) in the sequential filter differs significantly from that used in BWLS. Instead of time constants or segmented time constants, estimated parameters are modeled as stochastic sequences with configurable parameters to control both the amplitude and volatility of their evolution. While ODTK provides several stochastic sequence options (Johnson, 2013), the Vasicek sequence was selected for this effort. The Vasicek model (Vasicek 1977) originated in the financial community as an adaptation of the Ornstein-Uhlenbeck (Ornstein-Uhlenbeck 1930) model that modified a Weiner process describing Brownian motion to include particle friction. The technique is also known as the Langevin equation. It works by realizing that the motion will eventually trend toward a long term value (mean), while experiencing short term variations about that mean. The Vasicek model was designed to aid in the prediction of future trends in the bond markets. While perhaps not initially apparent, the incorporation of separate time periods and variability of the parameters allows the accurate modeling of dynamic variability of sensor observations and drag and solar radiation pressure variables. Glasserman (2004) shows the Vasicek model used for sequential orbit determination. The general equation for simulation of a Vasicek sequence includes both long term (drift) and short term (randomness) terms.

* ftp://cddis.gsfc.nasa.gov/pub/slr/data/npt_crd/. (Accessed Sep 2018)

$$
\begin{aligned}
V_{k+1} &= P_{k+1,k} V_k \;\; (1 - P_{k+1,k})\mu + \sqrt{1 - P_{k+1,k}^2}\, \frac{\sigma Z_{k+1}}{\sqrt{2a}} \\
a &= -\frac{\ln 0.5}{\tau_{1/2}} \\
P_{k+1} &= \exp(-a(t_{k+1} - t_k)) \\
\mu &= \lim_{(t_{k+1}-t_k)\to\infty} E\{V_k\} \\
\frac{\sigma^2}{2a} &= \lim_{(t_{k+1}-t_k)\to\infty} E\{(V_k - E\{V_{k+1}\})^2\}
\end{aligned}
\qquad (1)
$$

Here, μ is the long-term (LT) mean of the values (V_k), $\tau_{½}$ is the half-life, P_k is exponential transition correlation function, and σ is short-term (ST) standard deviation of the values. Z_k are random draws from a unit less normal distribution. The constant a introduces the half-life into the solution.

SATELLITE PHYSICAL CHARACTERISTICS

Satellite mass and area may be obtained from the ILRS website*. It's important to note that the size is of the array and not necessarily the entire satellite. For example, the 5 cm for GRACE could be misleading as the actual satellite is 1.942 m wide by 3.123 m long by 0.72 m high. For non-spherical satellites, such as GRACE, independent drag and solar pressure areas must be determined. The satellites used in this study are listed in Table 3 roughly in order of increasing orbital altitude.

Table 3: Satellite Physical Characteristics: NORAD SSC number and ILRS tracking numbers are given with the mass and area for each satellite. Solar radiation pressure is also provided with retroreflector and initial covariance information. Satellites are listed in increasing orbital altitude. All these satellites are spheres, so the atmospheric drag area is the cross-sectional (πr^2), while the solar radiation pressure could be the surface area ($4\pi r^2$). The solution for drag and srp are usually set to relative so all the sigmas are in percentages.

Satellite	NORAD #	ILRS #	Diameter (m)	Area (m^2)	Mass (kg)	Apogee Alt (km)	Perigee Alt (km)	*e*	*i* (°)	Retroreflector COM Offset (m)		
Larets	27944	304206	0.200	0.03142	23.280	691.0	675.0	0.001	98.00	0.000	0.000	0.000
Stella	22824	9306102	0.240	0.04524	48.000	806.0	795.0	0.001	98.90	0.000	0.000	0.000
STARLETTE	7646	7501001	0.240	0.04524	47.295	1107.0	805.0	0.021	49.80	0.000	0.000	0.000
LARES	38077	1200601	0.364	0.10406	386.800	1452.0	1436.0	0.001	69.50	0.000	0.000	0.000
Ajisai	16908	8606101	2.140	3.59681	685.000	1496.0	1479.0	0.001	50.00	0.000	0.000	0.000
LAGEOS 2	22195	9207002	0.600	0.28274	405.380	5952.0	5616.0	0.014	52.60	0.000	0.000	0.000
LAGEOS 1	8820	7603901	0.600	0.28274	406.965	5948.0	5838.0	0.004	109.90	0.000	0.000	0.000
Etalon 2	20026	8903903	1.294	1.31510	1415.000	19166.0	19078.0	0.002	65.30	0.000	0.000	0.000
Etalon 1	17951	8900103	1.294	1.31510	1415.000	19181.0	19070.0	0.002	64.20	0.000	0.000	0.000

It is important to properly model the location of the laser retro-reflector array (LRA) relative to the center-of-mass (COM) of the spacecraft. For spherical geodetic satellites, the center of mass is often located at the origin of the spacecraft body frame. For non-spherical satellites, such as GRACE, the location of the LRA relative to the center of mass is determined as the difference of the LRA and COM offsets measured in the spacecraft body frame. The LRA information for some spacecraft is more detailed, providing location information which is dependent upon the specific tracking methodology being used and the sensor to satellite geometry (Otsubo and Appleby, 2003). ODTK does not currently support these more refined models so an average LRA location is used. ODTK does provide the capability to estimate the LRA location. (See the following website for initial locations†).

Force model configurations are listed in Table 4. Note that the process noise in the table is for un-modeled accelerations. These terms insert additional process noise to the covariance to account for un-modeled accelerations in the radial, in-track, and cross-track directions. These accelerations may be due to a phenomenon such as outgassing or

* http://ilrs.gsfc.nasa.gov/missions/satellite_missions/current_missions/index.html. (Accessed Sep 2018)
† http://ilrs.gsfc.nasa.gov/missions/spacecraft_parameters/center_of_mass.html. (Accessed Sep 2018)

neglected forces such as albedo and smaller order effects. Adding process noise keeps the covariance from being unrealistically optimistic, and the larger covariance allows the filter to capture measurements after long times between observations. During the presentation at the conference, it was noted that LARES experienced m-level position uncertainty which were too high. This turned out to be IT and CT components of the additional process noise that were too high[*]. With corrected process noise values, the position uncertainty is now on the order of 10-15 cm.

Table 4: Satellite Force Model Configuration: The various force models are included, along with mass properties. A 70 × 70 geopotential was used for several satellites although some centers use a 40 × 40 field without significant changes. The satellites are roughly arranged from lowest orbital altitude to highest. Process noise is included for both acceleration and velocity units.

Force Models									
Parameter	**Larets**	**Stella**	**STARLETTE**	**LARES**	**Ajisai**	**LAGEOS 2**	**LAGEOS 1**	**Etalon2**	**Etalon1**
Gravity									
field size	70x70	70x70	70x70	70x70	70x70	70x70	70x70	40x40	40x40
Solid	yes	yes	yes	yes	yes	yes	yes	yes	yes
Time Dep	yes	yes	yes	yes	yes	yes	yes	yes	yes
Ocean	yes 4x0	yes 4x0	yes 4x0	yes 4x0	yes 4x4	yes 4x0	yes 4x4	yes 4x0	yes 4x0
Variational	8x8	8x8	8x8	12x12	8x8	6x2	6x2	12x12	12x12
Gen Rel	TRUE	TRUE	TRUE	TRUE	TRUE	TRUE	TRUE	TRUE	TRUE
Atmospheric Drag	yes	yes	yes	yes	yes	no	no	no	no
Third Body	yes	yes	yes	yes	yes	yes	yes	yes	yes
SRP	yes	yes	yes	yes	yes	yes	yes	yes	yes
Albedo	no	no	no	no	no	no	no	no	no
Thermal	no	no	no	no	no	no	no	no	no
Process Noise									
R (cm/s^2)	0.0000000	0.0000000	0.0000000	0.0000000	0.0000067	0.0000000	0.0000000	0.0000000	0.0000083
I (cm/s^2)	0.0000833	0.0000083	0.0000083	0.0000167	0.0000000	0.0000002	0.0000002	0.0000000	0.0000000
C (cm/s^2)	0.0000333	0.0000167	0.0000167	0.0000167	0.0000167	0.0000058	0.0000058	0.0000003	0.0000083
time int (min)	1	2	2	1	1	1	1	1	1
R (cm/s)	0.0000000	0.0000000	0.0000000	0.0000000	0.0004000	0.0000000	0.0000000	0.0000000	0.0000083
I (cm/s)	0.0005000	0.0005000	0.0005000	0.0001000	0.0000000	0.0000100	0.0000100	0.0000000	0.0000000
C (cm/s)	0.0020000	0.0010000	0.0010000	0.0008000	0.0010000	0.0003500	0.0003500	0.0000003	0.0000083

A difficult parameter to set is the retroreflector delay. These values are typically small, but physically, they represent the delay as the light is reflected back to the source. They can be modeled as either a range or a time. Values of a few cm in range are common. One approach used to estimate this parameter is to complete the initial sensor system setup, disable estimation of sensor biases and enable the retroreflector bias estimation. Given sufficient observations and proper initial setup, rough values may be established. We used a combination of this approach and values that had been previously determined for our study. The physical parameters needed to properly account for their dynamic behavior over time for each of the satellites are listed in Table 5.

SCENARIO INITIAL STATE SETUP

Initial Cartesian state vectors in the International Celestial Reference Frame (ICRF) were set from the previous scenario processing about 2 weeks of data through May and June 2018. We previously established that these orbits were in the couple cm range (Vallado, Woodburn, and Deleflie, 2014). Even with this level of accuracy, a short Least Squares run to modify the original orbit improved the results somewhat. In some cases, it makes sense to perform a filter and smoother run as the parameters are often close to estimates from previous SLR scenarios. All the new initial states were set to 1 Jun 2018 00:00:00.000.

[*] The process to determine acceptable process noise values is to examine the position uncertainty and the FSC test. As the process noise is decreased, the position uncertainty will decrease and the FSC will remain the about same until the process noise value is correct, at which point the FSC will begin to exhibit larger errors.

Table 5: Satellite Force Model Configuration: The various force models are included, along with area properties. Where possible, external sources were used to confirm our selections of mass and area (e.g. Rim et al. 2005). The satellites are roughly arranged from lowest orbital altitude to highest.

Parameter Settings									
Parameter	**Larets**	**Stella**	**STARLETTE**	**LARES**	**Ajisai**	**LAGEOS 2**	**LAGEOS 1**	**Etalon2**	**Etalon1**
Mass (kg)	23.28	48.000	47.295	386.80	685.00	405.380	406.985	1415.00	1415.00
Atmospheric Drag									
Model	Jacchia 71	NRLMSIS00E	NRLMSIS00E	Jacchia 71	Jacchia 71				
cd	3.06139	2.52738	2.5010	0.91782	2.6396				
area	0.03142	0.0452389	0.0452389	0.10406	3.59861				
LT Constant (BC	0.0045500	0.00238200	0.00239227	0.0003441	0.01348				
LT Sigma	0.05000	0.10000	0.10000	0.10000	0.10000				
LT Error Thresh	0.01000	0.01000	0.01000	0.01000	0.01000				
LT PNStep	0.00100	0.00100	0.00100	0.00100	0.00100				
ST Sigma	0.01500	0.10000	0.10000	0.10000	0.10000				
ST 1/2 life (min)	20	90	90	20	60				
Den 1/2 life	180	180	180	180	180				
Den Sigma Sc	1	1	1	1	1				
Use in Variationa	TRUE	TRUE	TRUE	TRUE	FALSE				
Addit PN	FALSE	FALSE	FALSE	FALSE	TRUE, .3/.3				
Solar Radiation Pressure									
area	0.03142	0.0452389	0.0452389	0.10406	3.59861	0.28274	0.28274	1.3151	1.3151
	1.036700	1.06000	1.01000	0.570000	1.01514	1.10680	1.12000	1.29000	1.25000
LT Sigma	0.1000	0.0500	0.0500		0.1000	0.0200	0.0400	0.0500	0.0500
LT Error Thresh	0.0050	0.0100	0.0100		0.0100	0.0100	0.0100	0.0100	0.0100
LT PNStep	0.0050	0.0010	0.0010		0.0010	0.0010	0.0010	0.0010	0.0010
ST Sigma	0.0200	0.1000	0.1000	0.0200	0.1000	0.0500	0.1000	0.1000	0.1000
ST 1/2 life (min)	20	360	360	7200	360	3600	3600	720	720
Use in Variationa	TRUE	TRUE	TRUE	TRUE	TRUE	TRUE	TRUE	TRUE	TRUE
Addit PN	TRUE, 1/1	FALSE	FALSE	FALSE	TRUE, .3/.3	TRUE, .5/.5	TRUE, .5/.5	TRUE, .15/.15	TRUE, .15/.15
Retroreflector									
LT Constant (m)	-0.430	-0.160	-0.160	-0.908	-1.966	-0.481	-0.481	-1.124	-1.124
LT Sigma		0.005	0.005		0.0010	0.005	0.005	0.0020	0.0020
LT Error Thresh		0.00050	0.00050		0.0010	0.000000001	0.000000001	0.000000001	0.000000001
LT PNStep		0.00005	0.00005		0.0010	0.000000001	0.000000001	0.000000001	0.000000001
ST Sigma	0.0500	0.005	0.005	0.0500	0.0100	0.050	0.050	0.0050	0.0050
ST 1/2 life (min)	525600	525600	525600	525600	259200	525600	525600	259200	259200
PhaseCenterX	0.0000	0.0000	0.0000	0.0000	0.0000	0.0000	0.0000	0.0000	0.0000
PhaseCenterY	0.0000	0.0000	0.0000	0.0000	0.0000	0.0000	0.0000	0.0000	0.0000
PhaseCenterZ	0.0000	0.0000	0.0000	0.0000	0.0000	0.0000	0.0000	0.0000	0.0000

Table 6: Satellite Initial State Vectors: State vectors are given for each satellite at the epoch of 1 Jun 2018 00:00:00.000.

	Position Vector (km)			Velocity Vector (km/s)		
Larets	957.9919084	-6181.1765781	3288.2041628	-1.6849360	3.2358986	6.5627432
Stella	-3397.2582450	5345.7669920	-3399.0594374	-0.7445126	3.6227844	6.4585448
STARLETTE	463.8778807	-4620.4077161	5478.1676363	7.5104990	0.3860784	-0.2558852
LARES	2447.9880935	-3796.0907087	6385.9465881	1.1538448	6.2382094	3.2674526
Ajisai	5003.4008471	-3817.8118021	4720.2007520	5.4892950	3.0050554	-3.3901303
LAGEOS-2	8879.3969171	-7942.6173000	-1419.4387532	2.7776272	2.2766584	4.5588460
LAGEOS-1	-2930.9772089	4101.2140612	11197.5697878	2.1064878	5.1155458	-1.3476615
Etalon-2	13514.2172928	20778.1822147	6145.2673751	-1.8909707	0.2093098	3.4594127
Etalon-1	-24970.7143166	4571.0780343	-2887.7711718	-0.7103178	-1.6317638	3.5223634

Due to the precise nature of the calculations, the latest Earth Orientation Parameter (EOP) and Space Weather (SPW) files are required for the best results. This is especially true when working with any LEO satellites (those satellites below about 1500 km altitude). An example demonstrates this later.

ODTK SENSOR SETUP

Sensor configurations in ODTK contain location information, as was described earlier, characterization of the sensor accuracy for producing various types of observations, and modeling information relevant to the treatment of the troposphere and ionosphere. Because the process of sensor characterization with sequential estimation differs from that of BWLS, we faced the challenge of determining initial values for the constant bias and sigma values required by the Vasicek formulation.

An internet search uncovered two tables that could help us form initial estimates*. However, recognize that the ST and LT values in these tables are for 3 month averages, and 1 year averages respectively. In our original formulation, these were used as initial starting values. The first table provides the single calibration values with STARLETTE, and LAGEOS RMS values. The RMS could be a surrogate for the White Noise Sigma (WNS), but the second table seemed better as it collects data from multiple Analysis Centers. Though not statistically rigorous, averaging the values gave reasonable initial results. The second table provides long and short term RMS for the last quarter from 5 analysis centers.

Because we had successfully run the filter for many years, we felt we could use the previous files with updated location, sensor eccentricities, etc. However, we really needed the statistical behavior of the observations over the entire period of time. The filter maintains some of this information internally in the restart records, but it was not easily accessible to examine and re-form the sensor parameters. Inspection of the specific restart records revealed that the LT sigma and biases had actually not varied much, so we initially kept these original values from the old sensor object. Several values are required for accurate characterization of each sensor.

- Constant Bias (a mean range bias per station). This value is generally found by averaging the residuals and it generally centers the observations about zero rather quickly.
- The long term sigma is used to characterize the uncertainty between the a priori constant value and the true mean of the range bias. The value may be found as the 1-2 sigma value of the measurement bias estimate from the filter. Usually 1 or 2 iterations will suffice to determine this value. It's good to keep this value a little high so the filter is able to make corrections during the runs. If it is set too low at first (as well as a ST sigma that is too low), changing the WNS will have no effect on the results.
- The short term sigma is used to characterize the serially correlated variations in the range bias about the mean and can be estimated from the variability of the residuals in the measurement bias report.
- The short term half-life is used to characterize the time scale over which short term variations occur. Approximate values are all that are needed. They should capture the approximate periodicity in the bias estimate.
- The white noise sigma (WNS) characterizes the amplitude of the random measurement noise. The value can be estimated from measurement residuals where the serially correlated bias effects have been removed. The WNS is *not* directly tied to the variability of the residuals in a particular run. For SLR observations, it ranges from about several mm to about 10 cm, describing the approximate accuracy of the individual sensor itself.
- The Vasicek formulation also requires ad-hoc machinery in ODTK to prevent the variance on the long term mean from going to zero. An error threshold for the long term mean root variance is specified along with a step increment of process noise. When the long term mean root variance falls below the threshold, process noise in the amount of the specified step is added. The selected values for the Error Threshold and PNStep are set based on the value of the constant bias term (10% and 1% respectively).

Using the above discussion, the sensor parameters were set as follows. The constant bias was set using the results of several filter/smoother runs and calculating the average offset (bias) in the residuals. The LT sigma was set to be 6 cm as we didn't see too much variation over a long period of time in the observations. The ST sigma was set to 15 cm as we have observed many large short term variations in the data (Fig. 2 and Fig. 6). It's unclear as to whether these are actual data, or artifacts of internal processing at the site. In general, we tend to use ST variations that are less than the LT (usually about 10% of the LT value), but this does not appear to be the case with the SLR data. The WNS was kept from the previous values, and was generally in the couple cm range.

For environmental modeling, the Marini-Murray troposphere model is used the model with a 0.01 m one-sigma uncertainty on the zenith delay and a 10 min half-life. Some stations specifically state that they do not include tropospheric variations, while others presumably do. Due to the high frequency of laser light, there is no need to model the effects of the ionosphere.

* https://ilrs.cddis.eosdis.nasa.gov/network/system_performance/global_report_cards/monthly/perf_201808_wLLR.html (Accessed Sep 2018)

RESULTS

An important consideration in performing the initial calibration is determining how many observations are available from each site for a particular satellite. Table 7 shows the observation distribution for the satellites of interest. Our processing didn't include all of the sensors listed in Table 1 because some sensors did not track the satellites we processed*.

Table 7: Satellite Observation Distribution: The number of observations during the study interval (June to August 2018) are given for each satellite under consideration. The green shaded cells indicate those with more than 1000 observations. The satellites are roughly arranged from lowest orbital altitude to highest. The total number of observations is given on the bottom line.

Larets			Stella			STARLETTE			LARES			Ajisai			LAGEOS 2			LAGEOS 1			Etalon1			Etalon2		
# obs	Site	Site #	# obs	Site	Site #	# obs	Site	Site #	# obs	Site	Site #	# obs	Site	Site #	# obs	Site	Site #	# obs	Site	Site #	# obs	Site	Site #	# obs	Site	Site #
1,208	ZIML	7810	1,948	YARL	7090	3,361	YARL	7090	3,695	ZIML	7810	4,528	YARL	7090	2,823	ZIML	7810	3,397	ZIML	7810	448	MATM	7941	481	YARL	7090
1,122	YARL	7090	1,787	ZIML	7810	2,821	ZIML	7810	2,283	YARL	7090	3,064	ZIML	7810	2,323	YARL	7090	2,536	YARL	7090	431	YARL	7090	305	MATM	7941
706	STL3	7825	1,146	STL3	7825	2,105	STL3	7825	1,895	HERL	7840	2,833	HARL	7501	1,921	MATM	7941	1,974	HERL	7840	199	WETL	8834	174	HARL	7501
660	GODL	7105	839	HARL	7501	1,855	MATM	7941	1,721	GRZL	7839	2,737	STL3	7825	1,543	HARL	7501	1,809	MATM	7941	179	HERL	7840	163	WETL	8834
538	GRZL	7839	684	GODL	7105	1,423	HARL	7501	1,547	POT3	7841	2,083	GRZL	7839	1,285	HERL	7840	1,251	HARL	7501	138	ZIML	7810	102	HERL	7840
476	HARL	7501	617	AREL	7403	1,416	GODL	7105	1,441	SOSW	7827	2,038	AREL	7403	1,046	GODL	7105	955	STL3	7825	109	GODL	7105	92	ZIML	7810
452	POT3	7841	497	GRZL	7839	1,376	GRZL	7839	1,381	MATM	7941	2,005	MONL	7110	922	STL3	7825	913	POT3	7841	91	HARL	7501	56	SOSW	7827
417	HERL	7840	487	MATM	7941	1,239	WETL	8834	1,176	HARL	7501	1,836	GODL	7105	662	WETL	8834	867	SISL	7838	87	SHA2	7821	33	THTL	7124
365	SIML	1873	483	WETL	8834	1,144	HERL	7840	1,171	GODL	7105	1,800	MATM	7941	600	SHA2	7821	805	GODL	7105	68	GRZL	7839	31	GRZL	7839
328	MATM	7941	369	POT3	7841	1,068	MONL	7110	1,066	STL3	7825	1,731	WETL	8834	458	SISL	7838	765	WETL	8834	63	SOSW	7827	25	SHA2	7821
320	CHAL	7237	325	HERL	7840	935	POT3	7841	821	WETL	8834	1,461	HERL	7840	424	HA4T	7119	733	SHA2	7821	45	CHAL	7237	24	STL3	7825
259	AREL	7403	318	CHAL	7237	839	CHAL	7237	810	SIML	1873	1,377	POT3	7841	394	GRZL	7839	576	GRZL	7839	36	BEIL	7249	14	KUN2	7819
224	WETL	8834	318	KTZL	1893	829	KTZL	1893	717	CHAL	7237	1,364	SISL	7838	376	CHAL	7237	539	MONL	7110	23	STL3	7825	11	GODL	7105
223	KTZL	1893	278	HA4T	7119	812	AREL	7403	639	MONL	7110	1,074	SHA2	7821	372	MONL	7110	527	HA4T	7119	21	SIML	1873	9	CHAL	7237
218	ALTL	1879	271	SIML	1873	698	SIML	1873	537	THTL	7124	985	KTZL	1893	310	THTL	7124	480	CHAL	7237	20	ALTL	1879	9	POT3	7841
218	HA4T	7119	253	HRTL	7503	662	SHA2	7821	463	SHA2	7821	893	CHAL	7237	307	BRAL	7407	458	THTL	7124	18	KUN2	7819	6	ALTL	1879
198	SISL	7838	242	SHA2	7821	535	SOSW	7827	461	HA4T	7119	851	HRTL	7503	287	POT3	7841	376	IRKL	1891	16	MDVS	1874	5	SIML	1873
177	HRTL	7503	230	SOSW	7827	518	HA4T	7119	446	BORL	7811	766	THTL	7124	243	SOSW	7827	346	GRSM	7845	15	MONL	7110	3	ARKL	1886
168	SHA2	7821	225	MONL	7110	509	SISL	7838	418	KTZL	1893	707	SOSW	7827	236	GRSM	7845	272	MDVS	1874	7	KOML	1868	3	BEIL	7249
142	SOSW	7827	191	SISL	7838	438	THTL	7124	355	SISL	7838	691	SIML	1873	211	SIML	1873	252	BEIL	7249	7	THTL	7124	3	IRKL	1891
141	BORL	7811	98	KUN2	7819	360	HRTL	7503	291	RIGL	1884	661	HA4T	7119	184	KTZL	1893	244	SOSW	7827	6	HRTL	7503	3	KOML	1868
135	RIGL	1884	81	IRKL	1891	336	BEIL	7249	253	ALTL	1879	541	BEIL	7249	180	BORL	7811	223	SIML	1873	6	IRKL	1891			
134	THTL	7124	71	BEIL	7249	219	GLSL	1824	232	BEIL	7249	362	KUN2	7819	179	BEIL	7249	212	BRAL	7407	6	POT3	7841			
125	MONL	7110	63	ZELL	1889	200	ZELL	1889	232	IRKL	1891	357	RIGL	1884	165	BAIL	1887	192	ALTL	1879	5	ARKL	1886			
92	BADL	1890	62	THTL	7124	180	BORL	7811	227	MDVS	1874	307	GLSL	1824	147	IRKL	1891	186	BAIL	1887	2	SEJL	7394			
72	KUN2	7819	48	SVEL	1888	179	KUN2	7819	225	AREL	7403	295	ZELL	1889	136	ALTL	1879	143	ARKL	1886						
58	SEJL	7394	27	SEJL	7394	122	SEJL	7394	204	BADL	1890	229	BORL	7811	135	MDVS	1874	135	KTZL	1893						
57	GLSL	1824	26	ARKL	1886	119	RIGL	1884	199	ZELL	1889	219	ARKL	1886	117	HRTL	7503	131	KUN2	7819						
56	BEIL	7249	9	BRAL	7407	116	ARKL	1886	186	ARKL	1886	207	IRKL	1891	98	AREL	7403	113	HRTL	7503						
53	KOML	1868	7	GRSM	7845	103	IRKL	1891	162	KUN2	7819	109	BRAL	7407	97	ZELL	1889	110	BORL	7811						
43	ZELL	1889	6	BORL	7811	54	MDVS	1874	145	HRTL	7503	108	SEJL	7394	89	ARKL	1886	88	KOML	1868						
28	SVEL	1888	6	RIGL	1884	43	BRAL	7407	112	KOML	1868	68	MDVS	1874	88	KUN2	7819	81	RIGL	1884						
20	IRKL	1891				28	SVEL	1888	98	GLSL	1824	52	SVEL	1888	74	SEJL	7394	72	AREL	7403						
16	BAIL	1887				21	MDOL	7080	89	SEJL	7394				55	KOML	1868	61	ZELL	1889						
10	BRAL	7407							69	GRSM	7845				55	SVEL	1888	42	SEJL	7394						
									63	SVEL	1888				31	RIGL	1884	37	BADL	1890						
									35	BRAL	7407				17	BADL	1890	13	SVEL	1888						
9459			12012			26663			25865			38339			18590			21914			2046			1552		

We use 3 primary graphs to illustrate the performance of each run – residual ratios, position uncertainty, and filter smoother consistency. There are many other available reports and graphs in ODTK, but these 3 provide an immediate insight into orbit determination performance.

The first plot to consider is the residual ratios (residuals divided by the standard deviations) that normalize all types of data, and show if most of the data is within a ±3 band as expected for normally distributed residuals. The original processing from the month of June is shown below – notice the large vertical spikes in the data. This was an indication that an update to the sensor configurations was needed!

* For ODTK use, to include updates to a sensor that was not included in the original processing, several steps are recommended. First, the original sensor file (.tso) should be modified with the relevant parameter changes (usually the constant bias) so that any new scenarios can use the latest information. For scenarios using the .tso file with restart records, you can manually change the sensors characteristics and then select the Stochastic Model Update (SMU) and the object settings. This will let the filter accept the change at the epoch time of the restart. Subsequent later restart runs of the scenario will use the change (and any variations resulting from processed observations), the objects displayed settings will not revert to the value stored in the restart record. Note that re-running the scenario without this SMU setting from the epoch time will not include the change as it reverts to the value stored in the restart record at the epoch time. The change is only effective after the original time.

Another way to deal with sensors that are not used initially but come into play later is to use the dynamic state space option for measurement biases. With this option on the initial run, the tracking data is scanned prior to the filter running and only tracking bias states for which measurements exist are added to state space. On subsequent runs from restart records, biases associated with trackers whose measurements are seen for the first time will be added into the state space and trackers with no additional measurements and whose bias states have de-correlated from the rest of the state will be dropped.

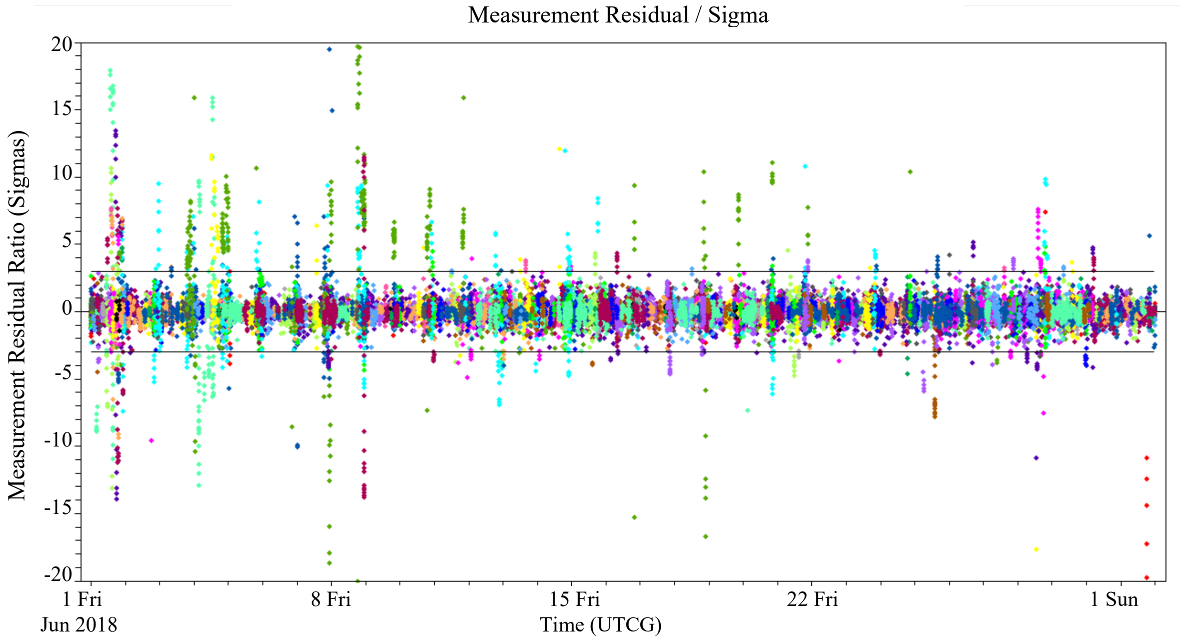

Figure 2: Residual Ratio Plot – Original configuration: The residuals divided by the residual root variances provide a normalized look at the observations and processing. Results should fall within a ±3 band.

The next plot is the covariance (uncertainty) in the orbit as the filter processes the data. Note that the uncertainty estimate is updated as each observation is processed.

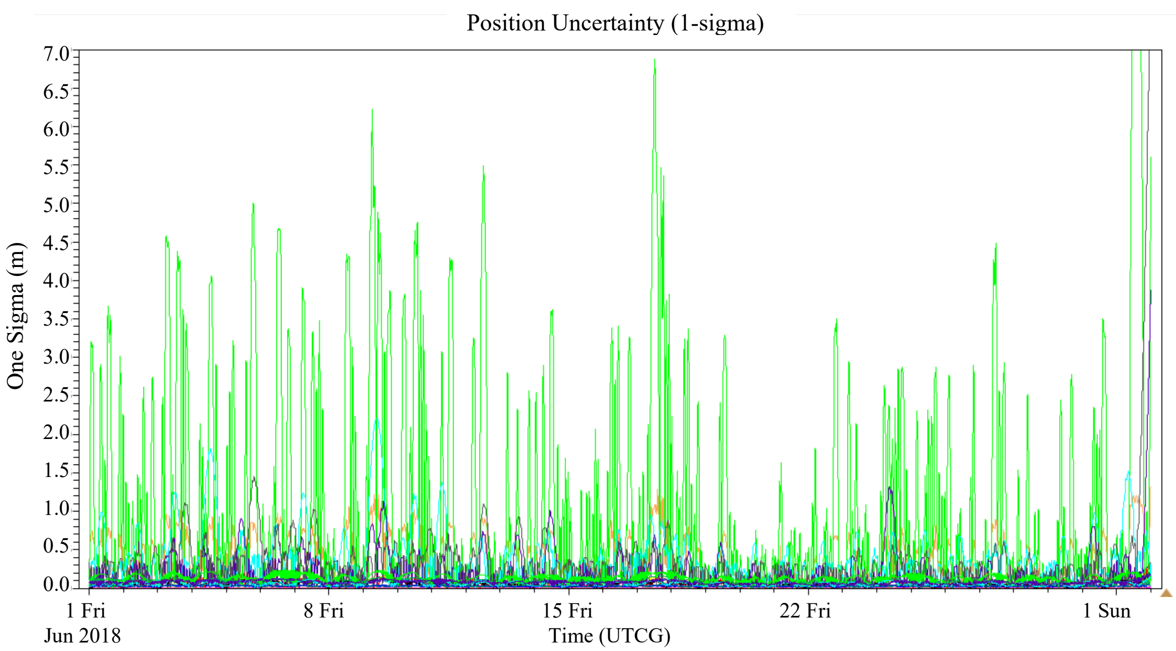

Figure 3: Position Uncertainty (Covariance) Plot – Original configuration: Note that with a filter, the estimate of the uncertainty changes with each observation. The LARES satellite has the largest uncertainty.

Figure 4 shows the uncertainty information for the remaining satellites once the uncertainty information from LARES (it had the largest uncertainty) has been removed.

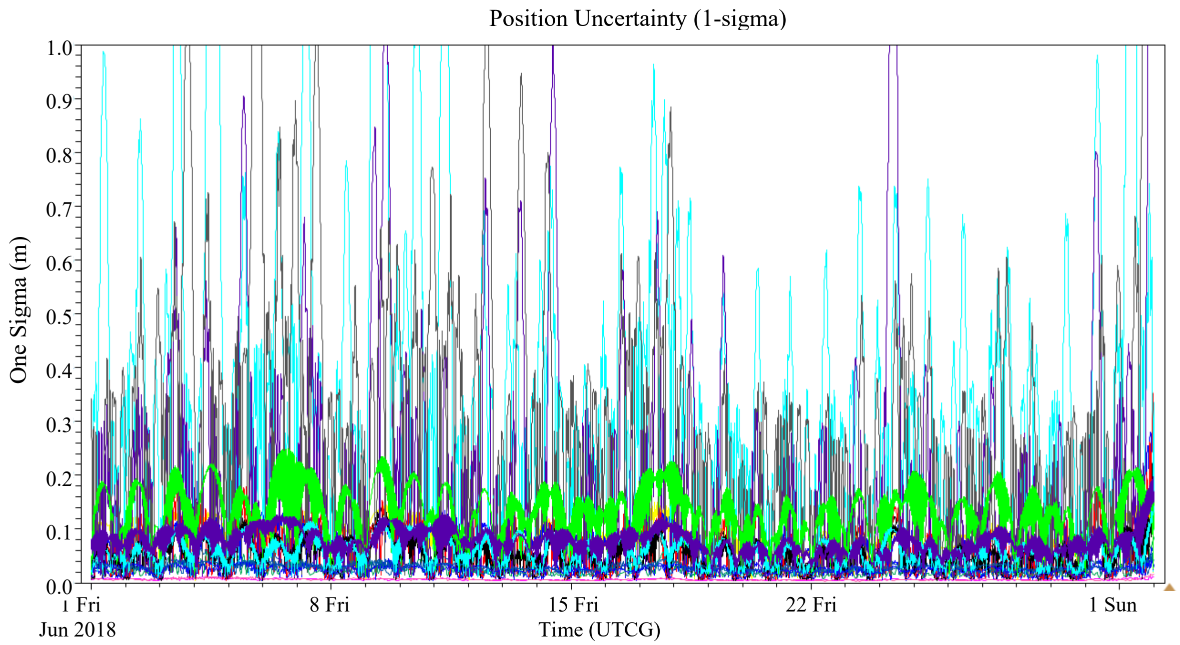

Figure 4: Position Uncertainty (Covariance) Plot – Original configuration: Note that with a filter, the estimate of the uncertainty changes with each observation. This plot shows Ajisai, LAGEOS 1 and LAGEOS 2, Larets, STARLETTE, and Stella.

The final graph is the Filter-Smoother Consistency (FSC) test which highlights any differences between the filter and smoother runs. This test in particular is important as it will show (and magnify) any incorrect setups parameters in the force models, observational data, sensors, etc.

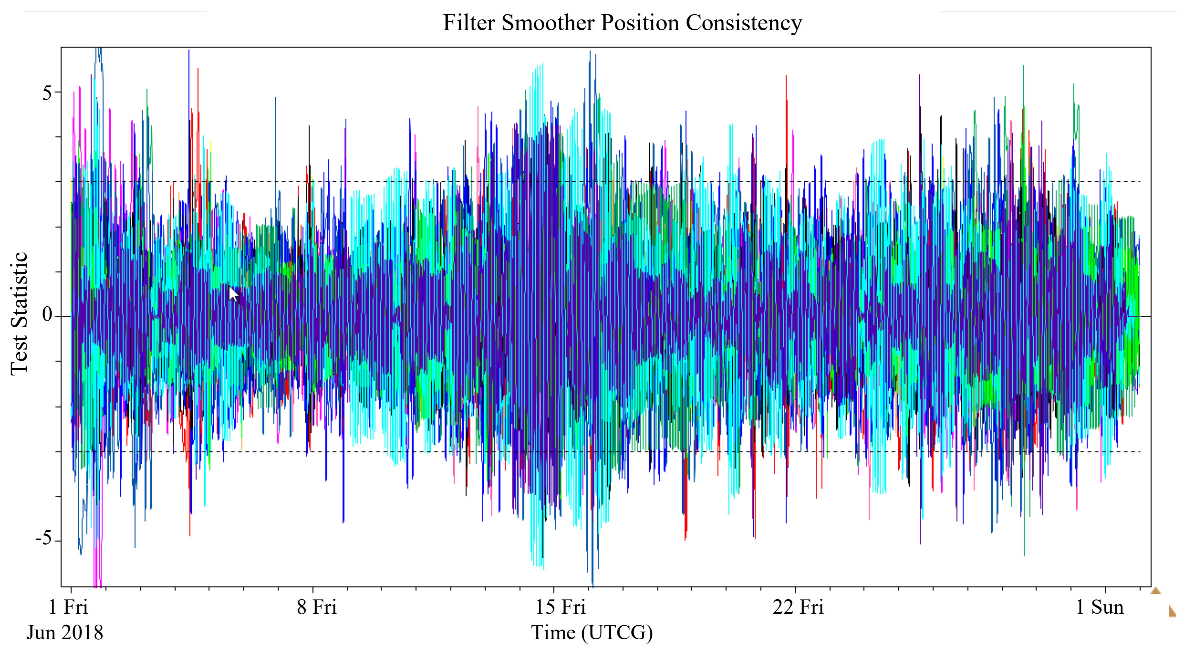

Figure 5: Filer-Smoother Consistency (FSC) Plot – Original configuration: Perhaps the most sensitive plot to examine, the FSC will indicate if force models, sensor parameters, EOP, etc are not correctly setup. Results should fall within a ±3 band.

Now that we have processed large quantities of observational data, our initially assumed constant bias values can be updated based on the residual information. The FSC tests indicated that LAGEOS 1 needed a little more un-modeled process noise in the cross-track direction (0.000 000 25 to 0.000 000 58 cm/s^2). This is likely due to un-modeled forces like those discussed in Duha (2001) on thermal re-radiation effects on the satellites. The updated results look similar to those generate above, but had some notable differences. Notice how much cleaner the residual ratios are with all the sensors represented, and with updated parameters, although there are still vertical spikes in the data. In particular, sensor SEJL seemed to have greater variability in the residuals, so we increased the measurement uncertainty.

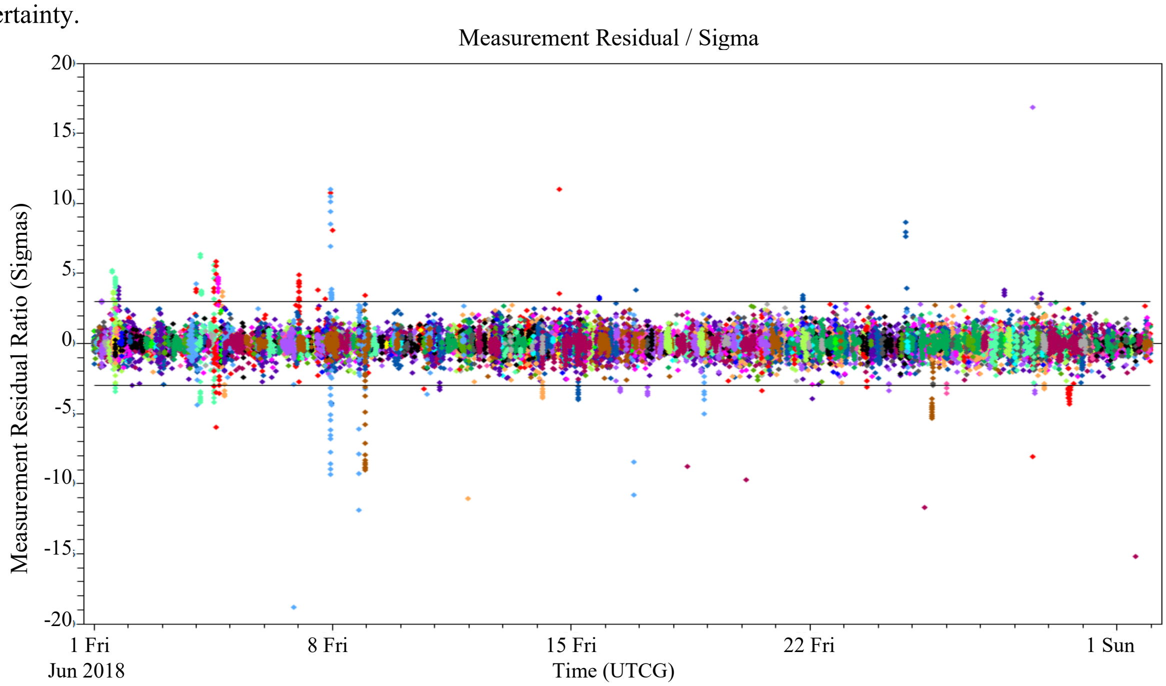

Figure 6: Residual Ratio Plot – New configuration: The results are much better than the previous run but there are still a few vertical looking residual passes.

Looking at the residuals only, we see normal results.

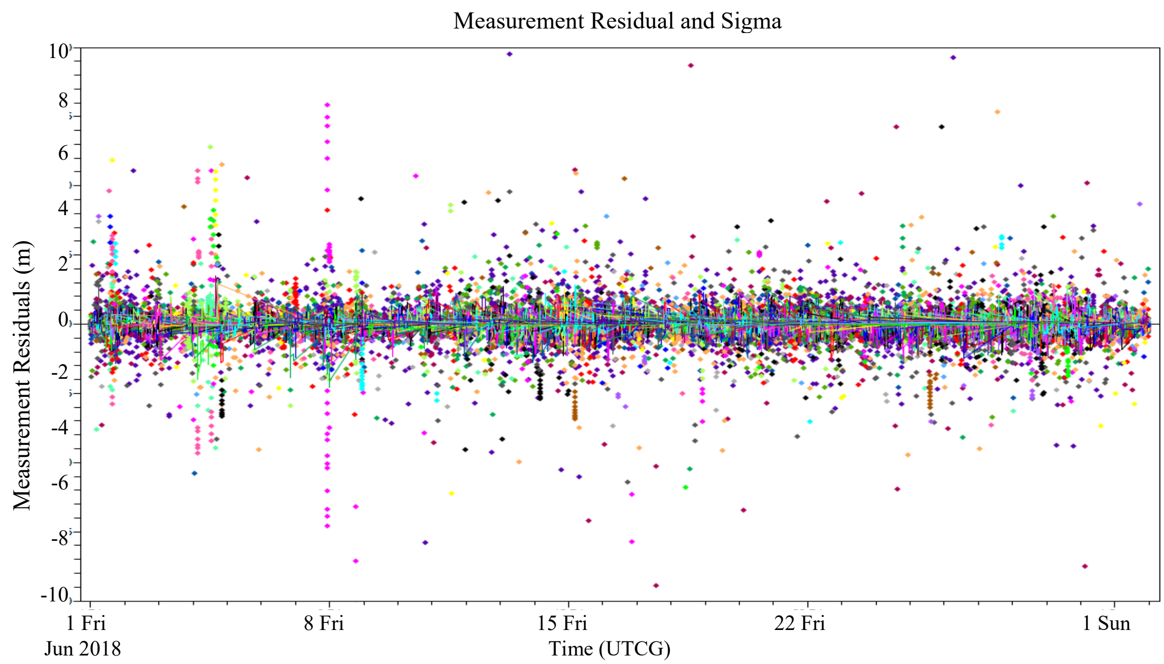

Figure 7: Residual Plot – New configuration: The results look normal, with some outlier observations, but most residuals well under a meter.

The position uncertainty is very similar, as expected, since the uncertainty is mainly driven by the number of accepted measurements. While the number of rejected measurements has decreased, the increased in accepted measurements is still a small percentage of the overall number of observations.

The position uncertainty now looks like the original configuration, but now *includes* LARES and the Etalon satellites.

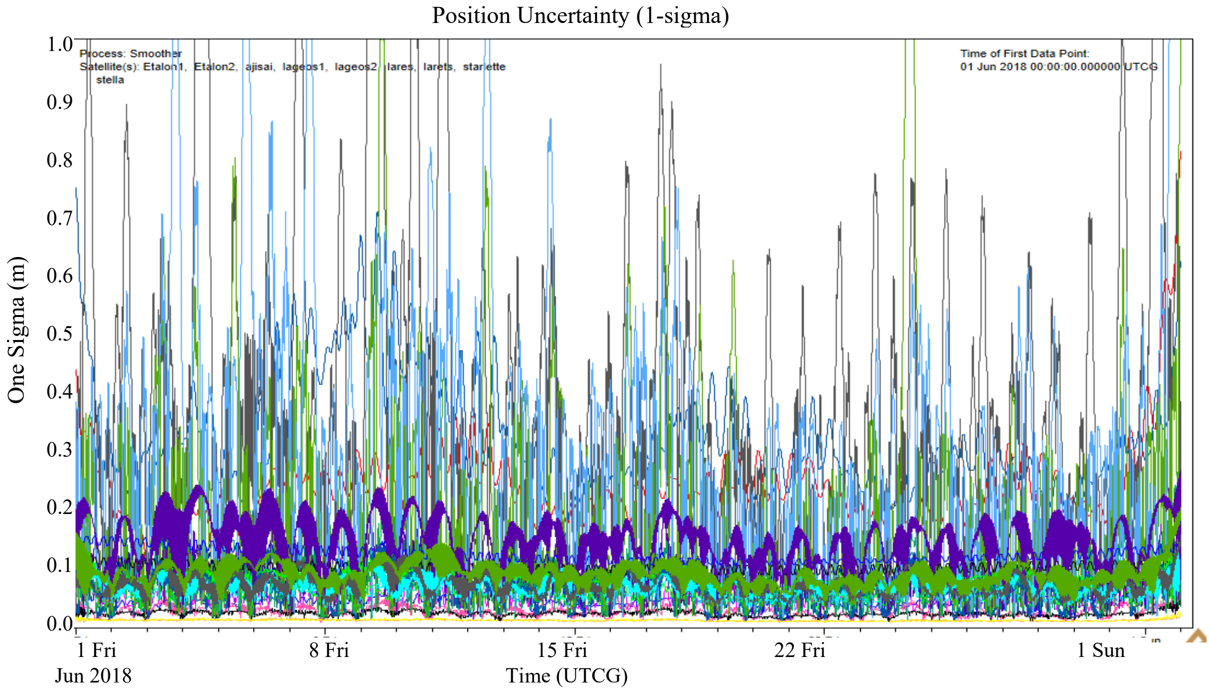

Figure 8: Position Uncertainty (Covariance) Plot – New configuration: Note the improved performance from the original formulation. This plot shows Ajisai, Eatlon 1 and Etalon2, LAGEOS 1 and LAGEOS 2, LARES, Larets, STARLETTE, and Stella.

It's useful to examine each component of the position uncertainty. The radial component, as expected due to the accuracy of the SLR data, has the best performance. Notice that the scale for Radial is smaller than for in-track and cross-track.

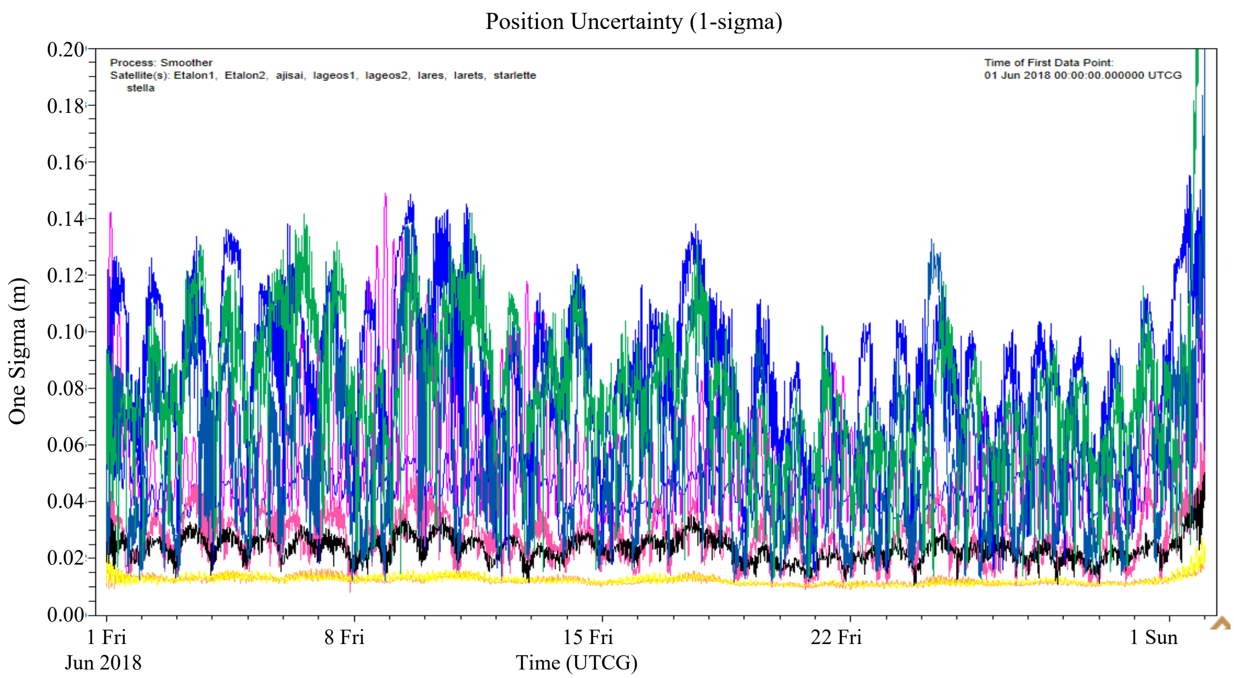

Figure 9: Radial Position Uncertainty (Covariance) Plot – New configuration: The radial position uncertainty is the best because the SLR observation is the most accurate in the range direction.

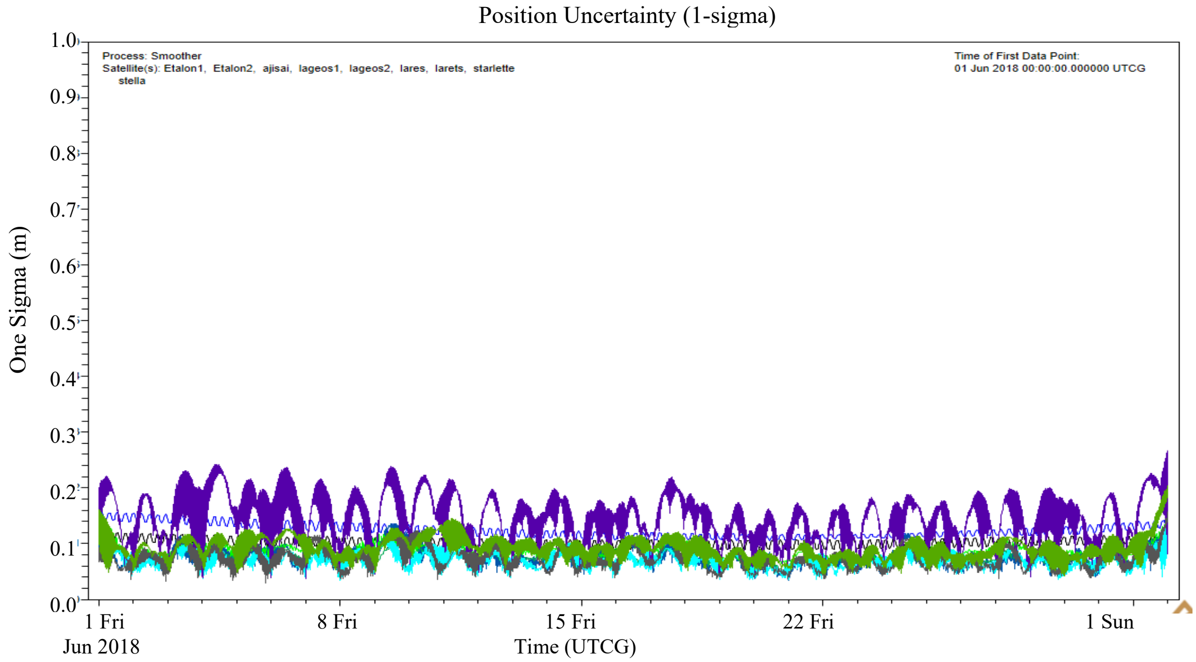

Figure 10: Cross-track Position Uncertainty (Covariance) Plot – New configuration: The cross-track position uncertainty is relatively small, but worse than the radial. The worst performance is for Larets, Etalon 1 and Etalon2, Starlette, and Stella.

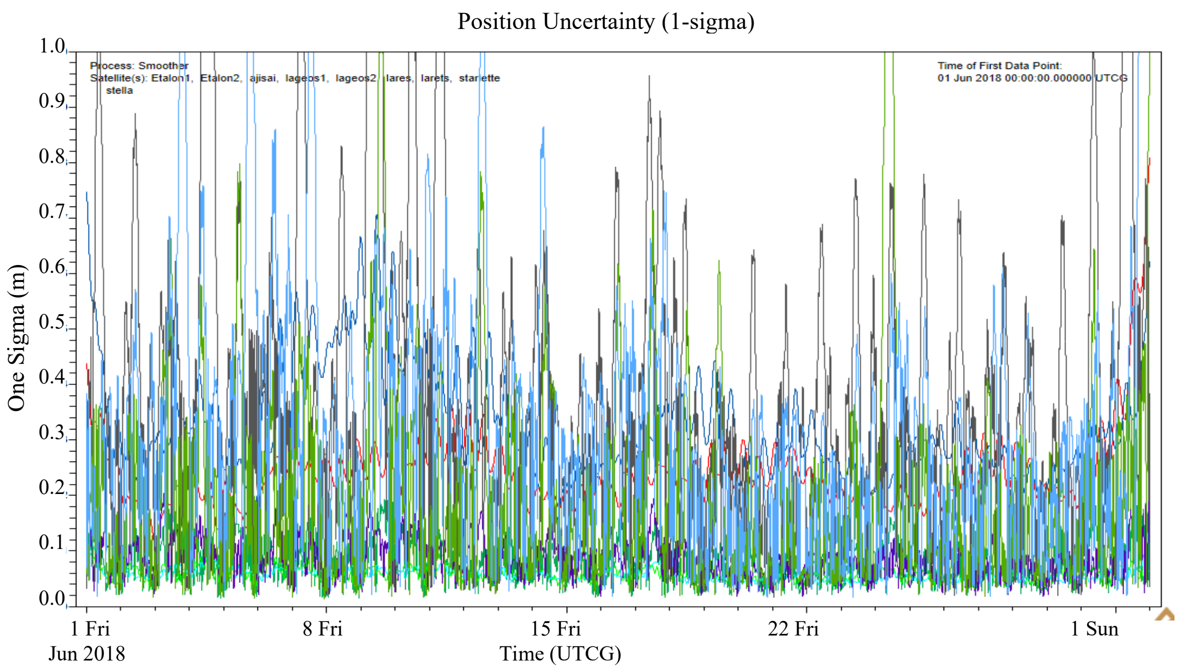

Figure 11: In-track Position Uncertainty (Covariance) Plot – New configuration: The in-track position uncertainty is the largest uncertainty component. The worst performance is for Larets, Starlette, and Stella. This is not unexpected because the in-track direction experiences the effects of atmospheric drag.

The FSC is similar to the original, but has a little more variation after about the middle of the month.

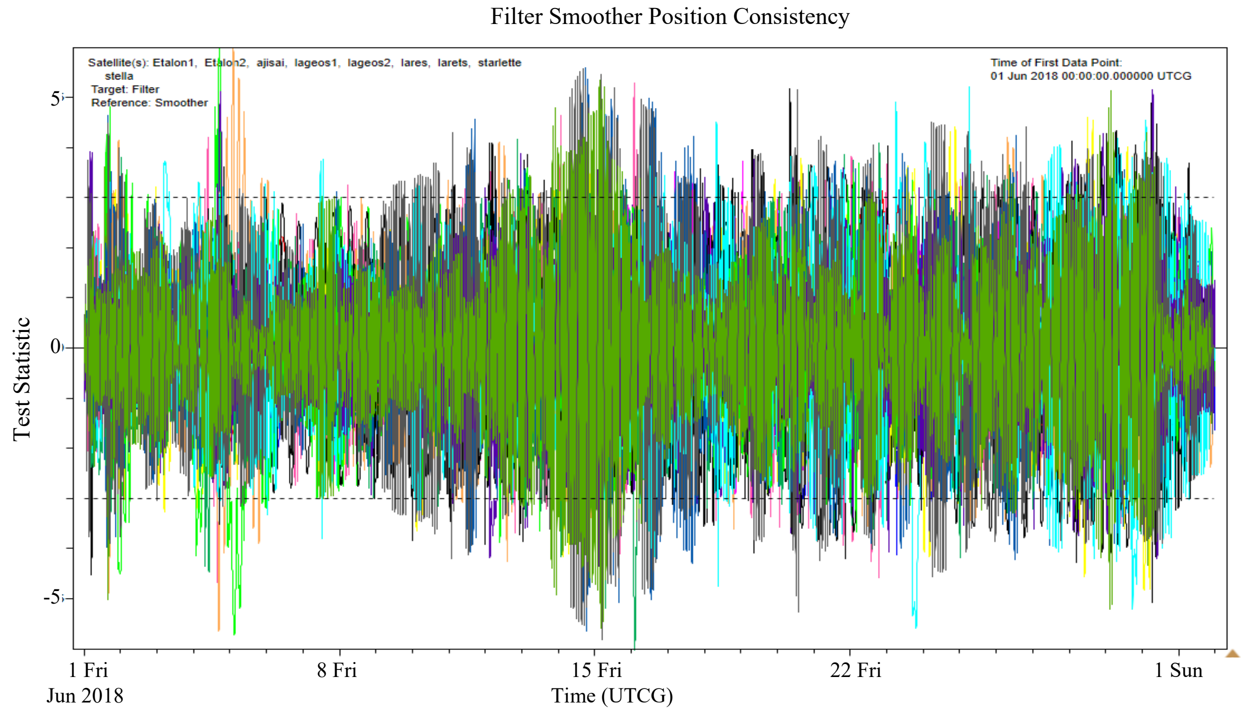

Figure 12: Filer-Smoother Consistency (FSC) Plot – New configuration: The results for the FSC look very similar to the previous setup.

As an aside, we note that with an older EOP file, the FSC picked up the inconsistency and showed larger variations after the first week in June where the old EOP file had ended with actual data. The remaining reports and graphs showed no difference. This highlights the importance of examining the FSC report, and of updating EOP and Space Weather data prior to the orbit estimation process!

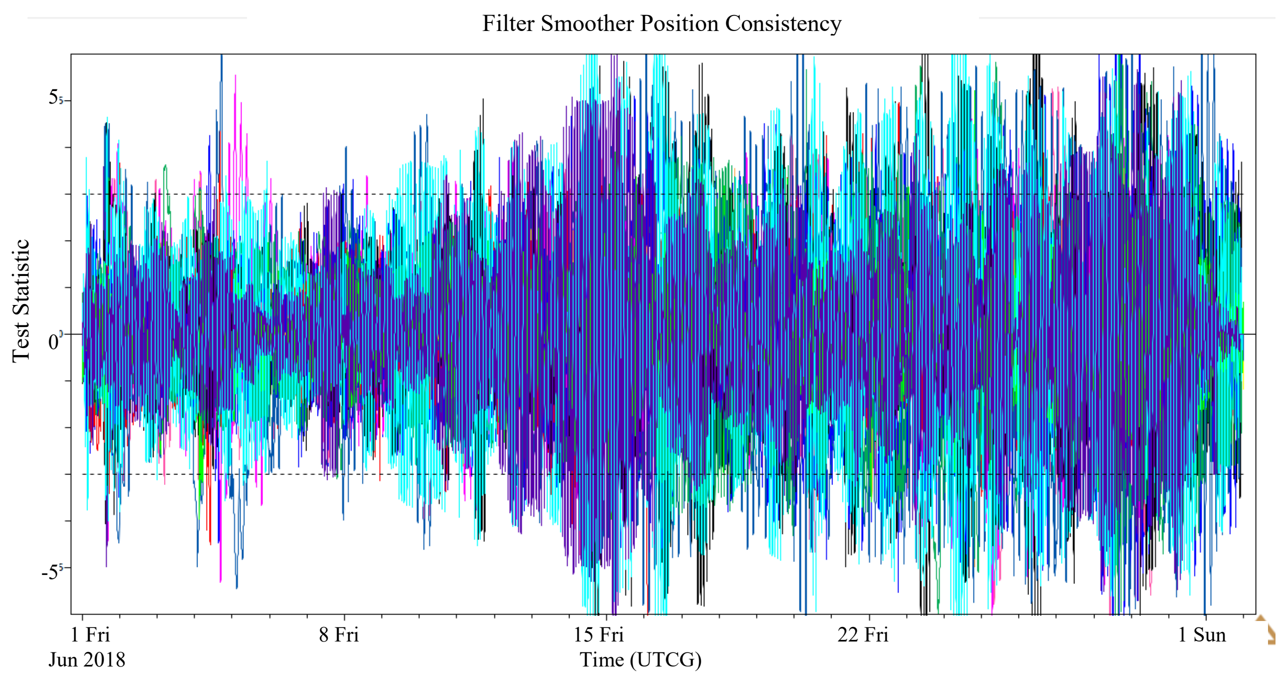

Figure 13: Filer-Smoother Consistency (FSC) Plot – New configuration, old EOP data: The FSC is very sensitive to several parameters in the OD processing. Notice the increased variation after about 8 June 2018 where the actual data ended (compared to Fig. 12).

Comparing the two ephemerides (original and new configurations), we find sub meter-level differences. All the plots have the same scale except for LARES.

LARETS Position Differences (new – old, m)

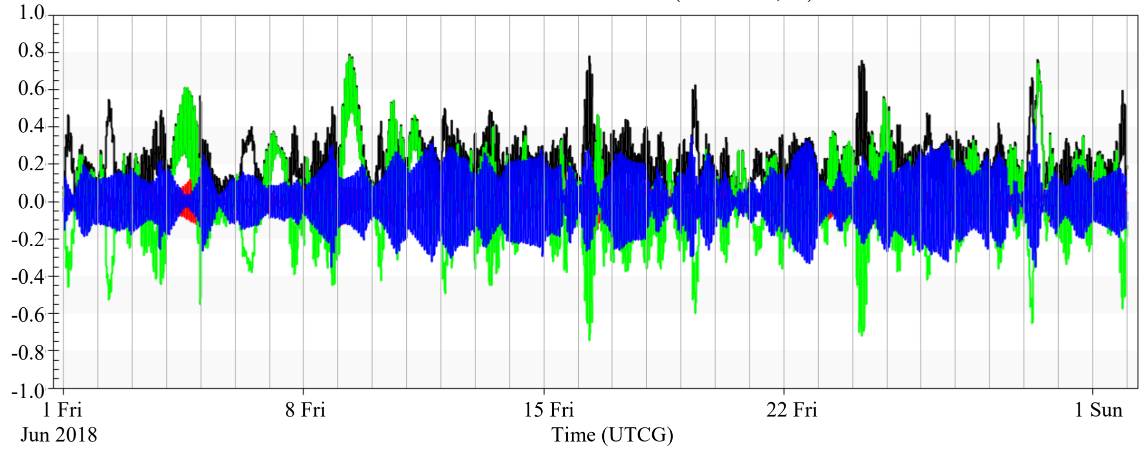

Stella Position Differences (new – old, m)

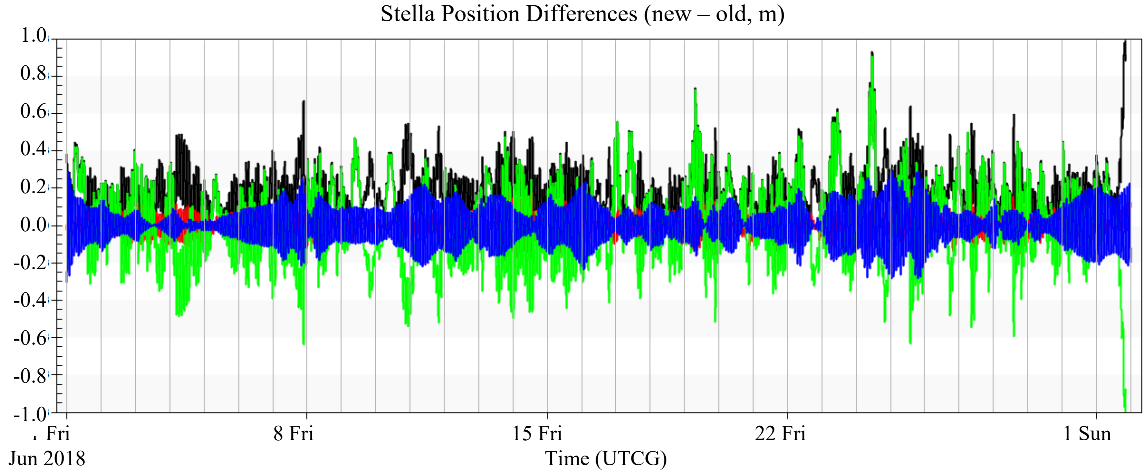

Starlette Position Differences (new – old, m)

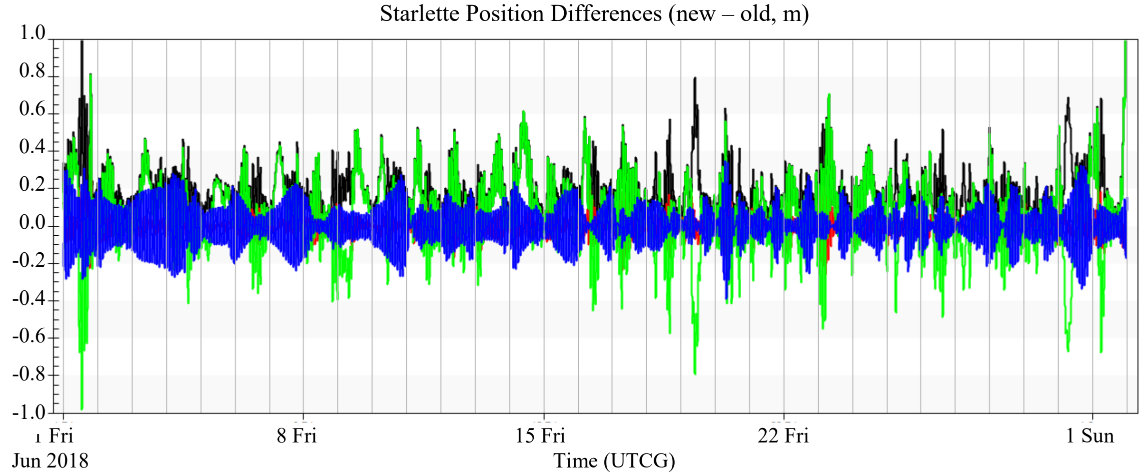

Note the change of scale:

LARES Position Differences (new – old, m)

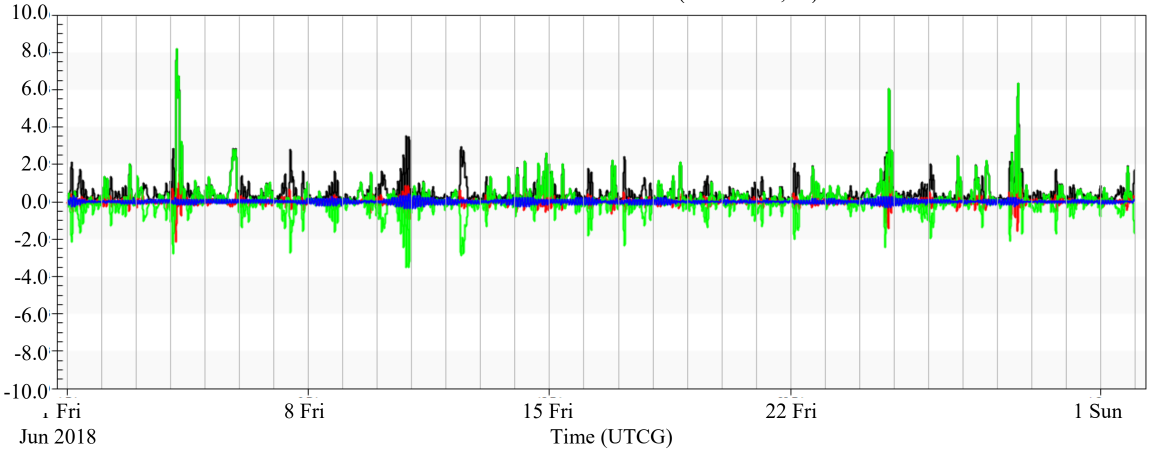

Ajisai Position Differences (new – old, m)

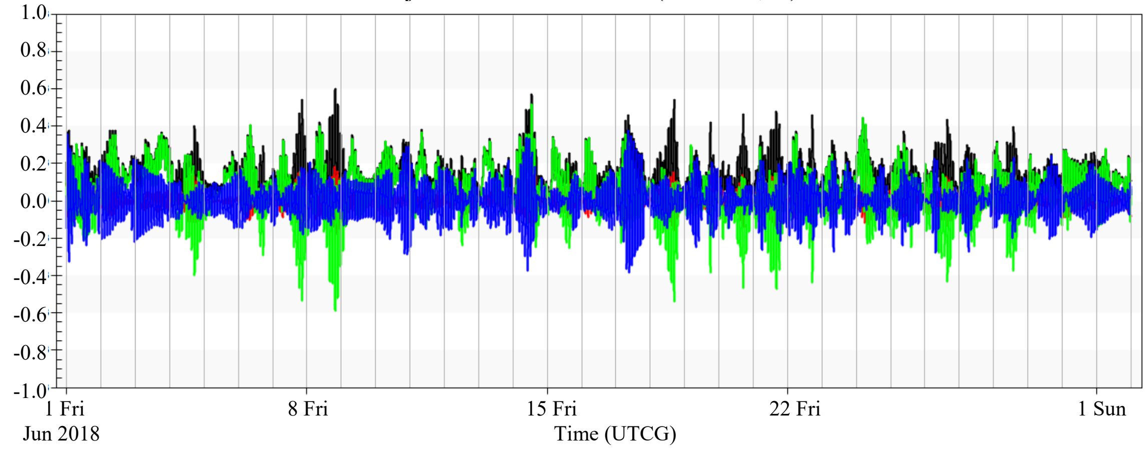

LAGEOS 2 Position Differences (new – old, m)

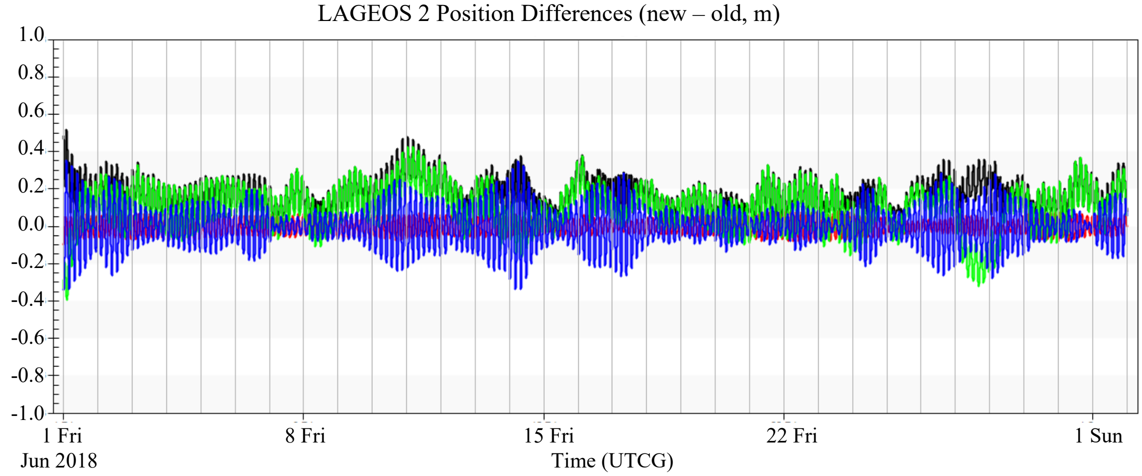

LAGEOS 1 Position Differences (new – old, m)

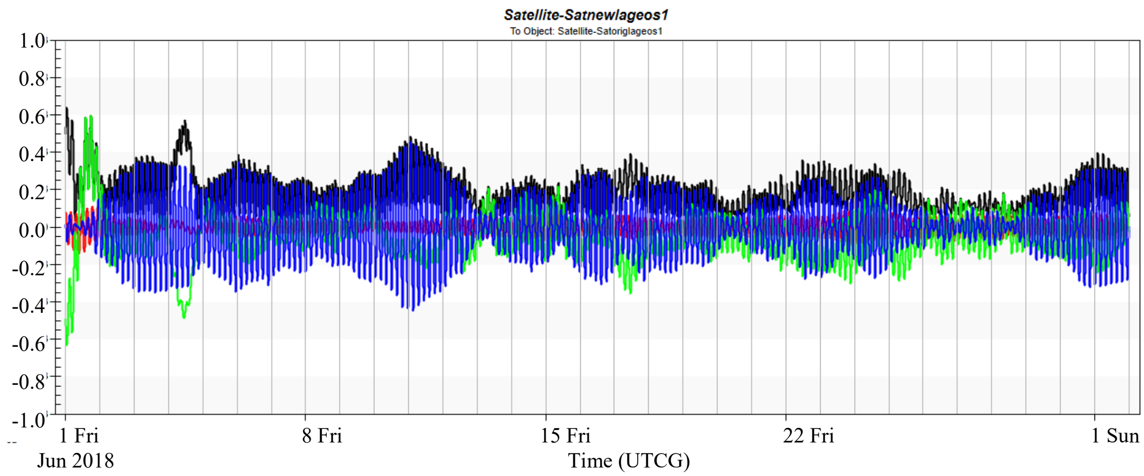

Etalon 2 Position Differences (new – old, m)

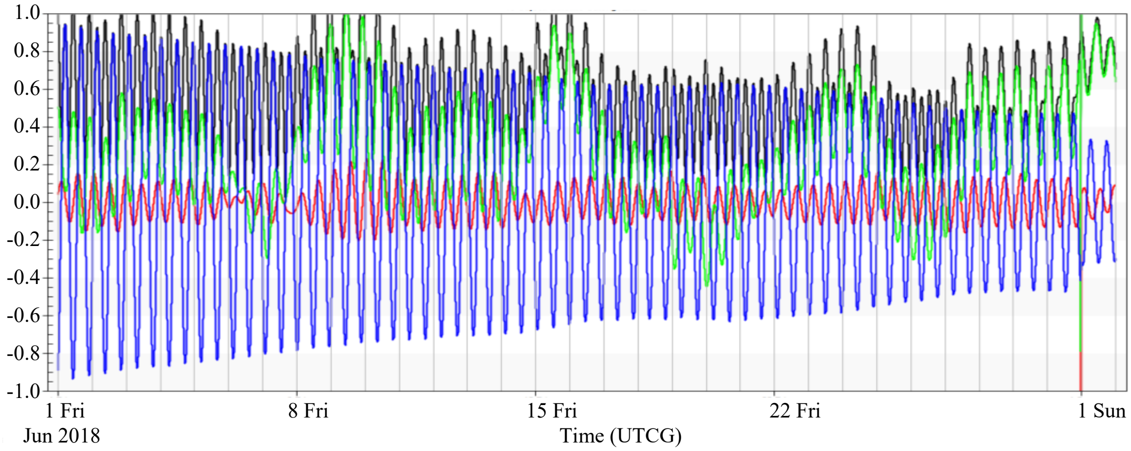

Etalon 1 Position Differences (new – old, m)

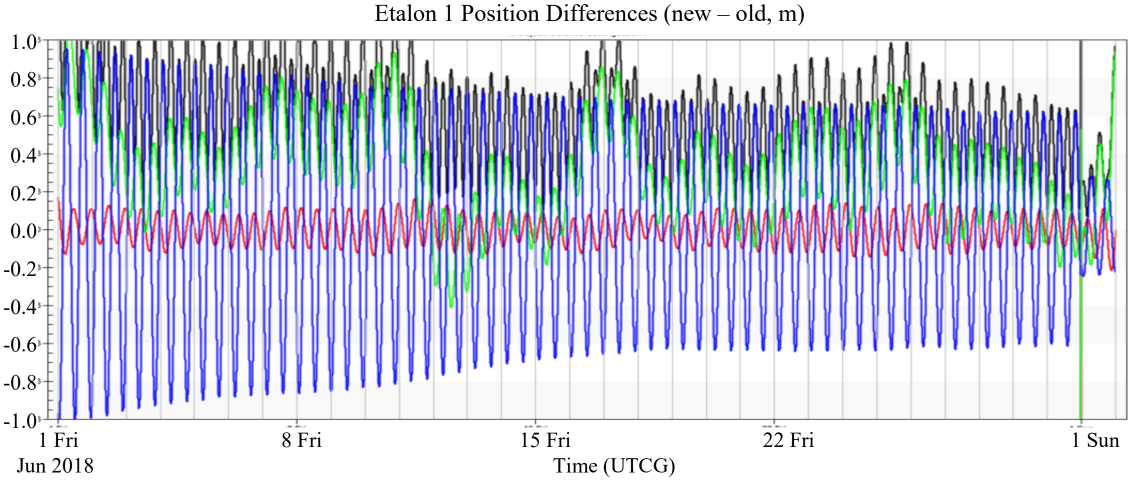

Figure 14: Position Comparison: The original configuration and the new formulation show minor differences through the month of June 2018. With less observations, we expect the Etalon orbits to be a little less accurate. The plots are roughly arranged from lowest orbital altitude to highest.

The final SLR sensor file for ODTK is available upon request from the authors.

COMPARISONS TO CPF PREDICTED ORBITS

An additional check was included using the Consolidated Predicted File (CPF) formats*. These are predicted orbits, so the accuracy is generally less than rigorous OD solutions of the SLR data, but they do afford a comparison at about the meter-level. There are several centers that produce the ephemerides†. For a few SLR satellites, comparing the CPF from August to October 2018 to the new SLR-derived solution, we find generally about 15 meter level differences, but there were some exceptions

Larets Position Differences (new – CPF, m)

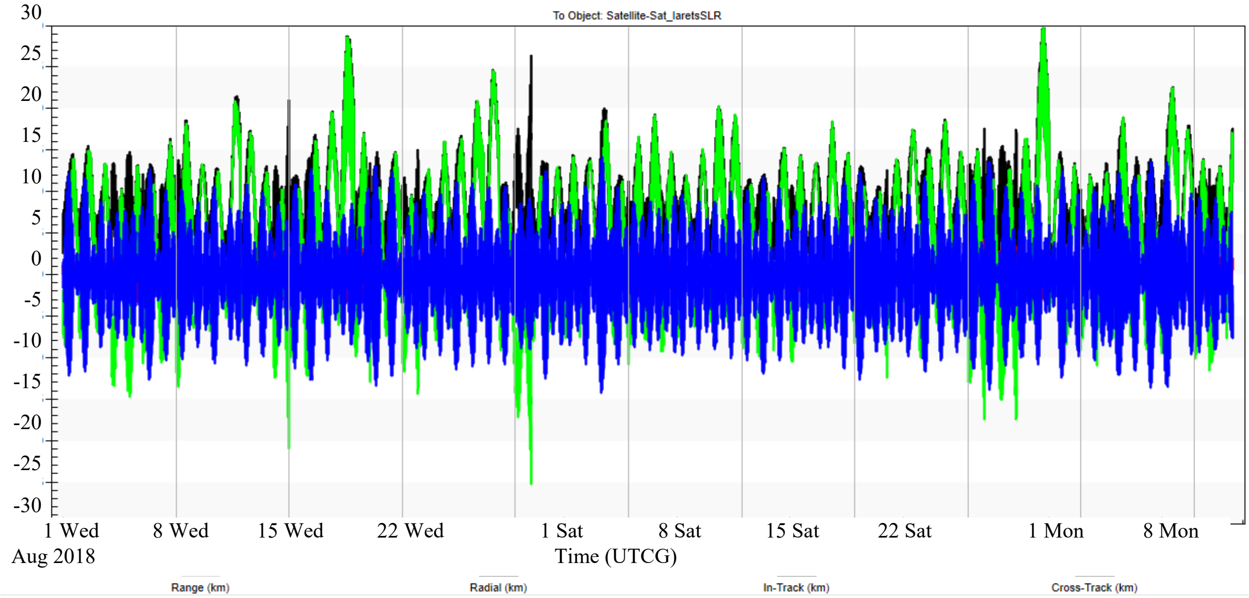

Stella Position Differences (new – CPF, m)

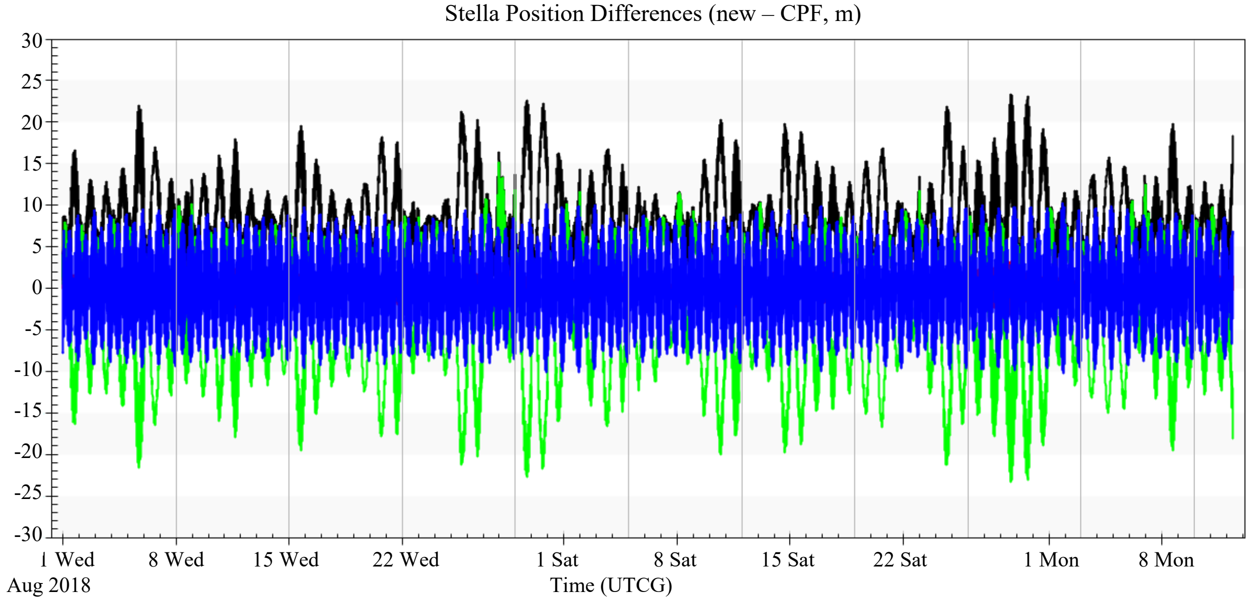

* ftp://cddis.gsfc.nasa.gov/pub/slr/cpf_predicts/ (accessed Sep 2018).
† https://ilrs.cddis.eosdis.nasa.gov/data_and_products/predictions/prediction_centers.html (Accessed Oct 2018).

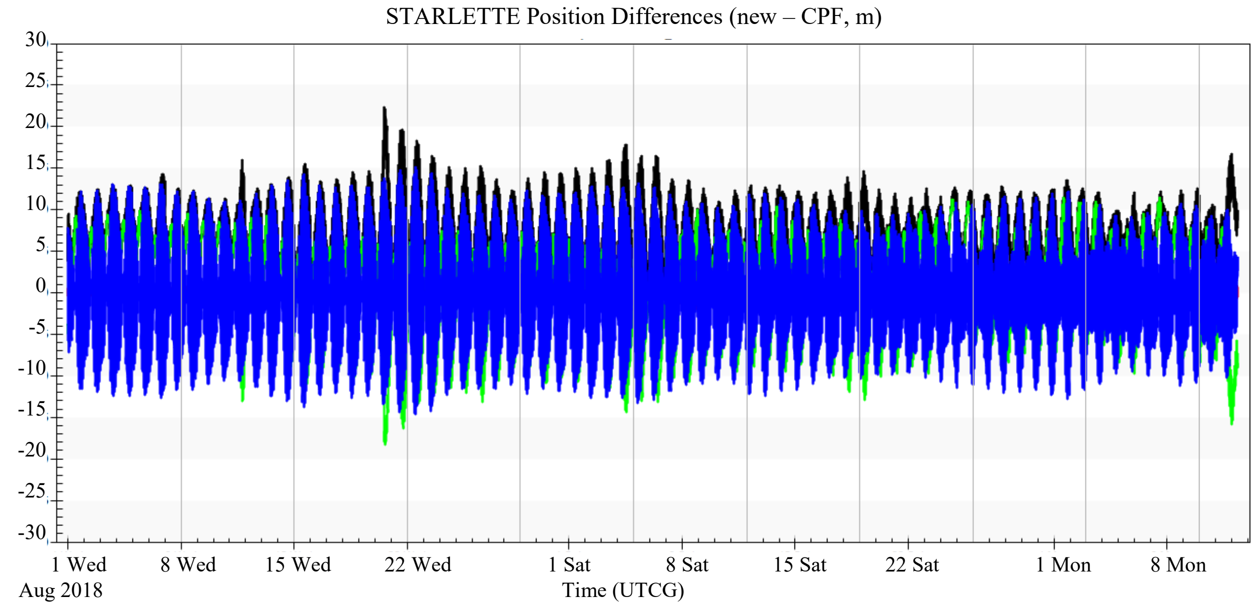
STARLETTE Position Differences (new – CPF, m)
30
25
20
15
10
5
0
-5
-10
-15
-20
-25
-30
1 Wed
Aug 2018
8 Wed
15 Wed
22 Wed
1 Sat
8 Sat
15 Sat
22 Sat
1 Mon
8 Mon
Time (UTCG)

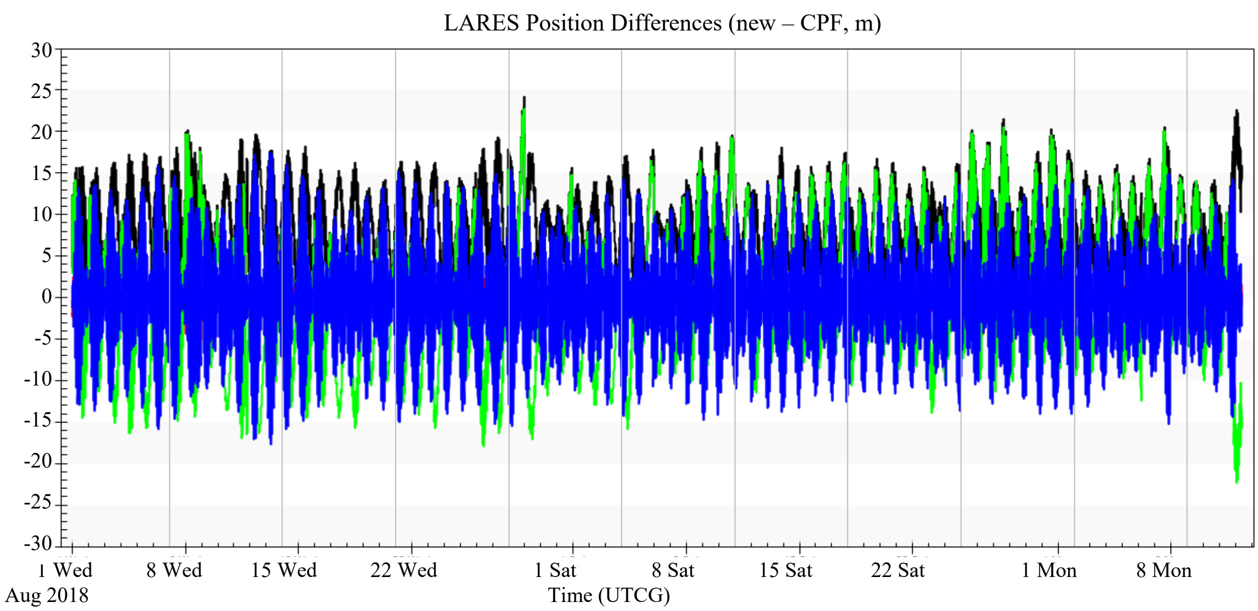
LARES Position Differences (new – CPF, m)
30
25
20
15
10
5
0
-5
-10
-15
-20
-25
-30
1 Wed
Aug 2018
8 Wed
15 Wed
22 Wed
1 Sat
8 Sat
15 Sat
22 Sat
1 Mon
8 Mon
Time (UTCG)

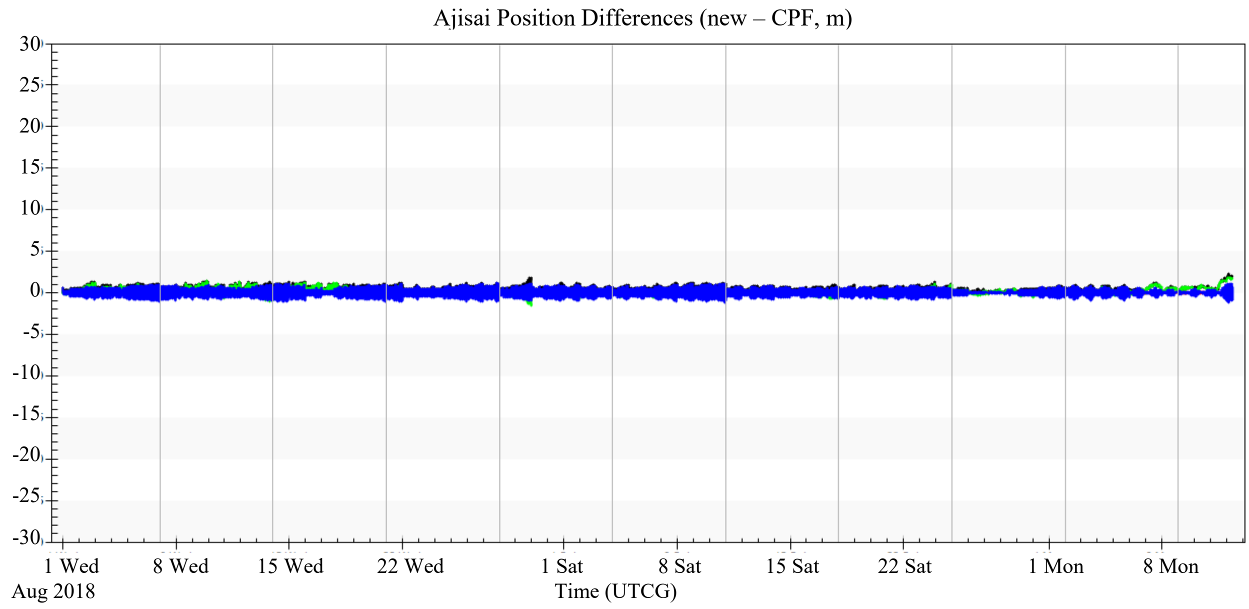

Note the change of scale for Etalon1:

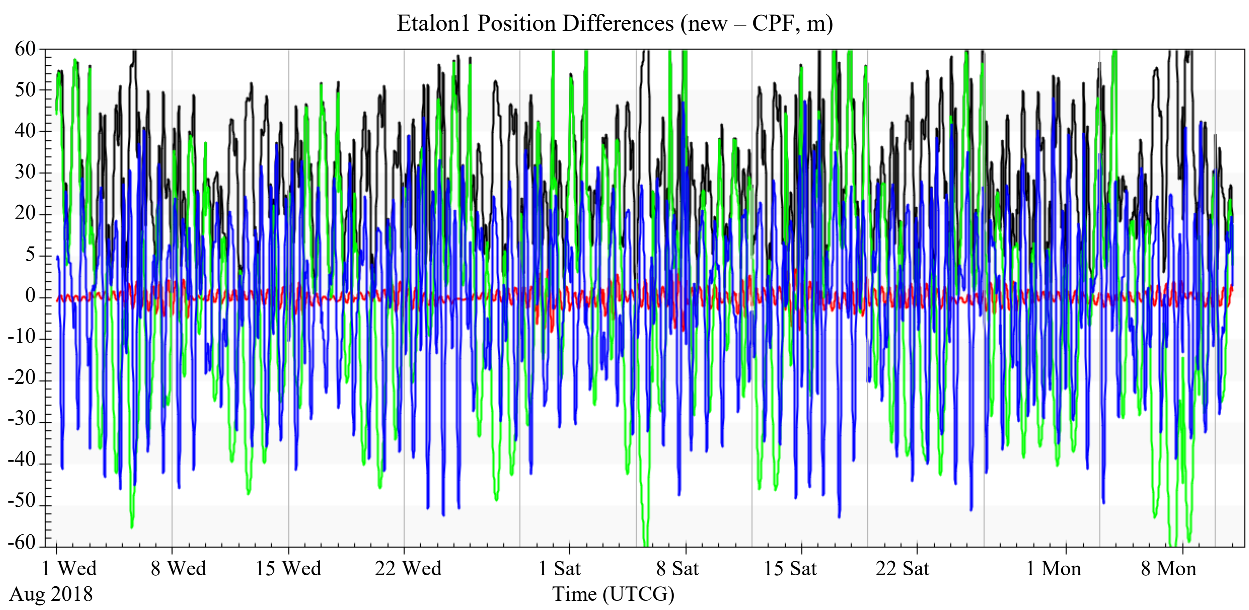

Figure 15: Comparison to CPF orbits: The plots show positional differences between the CPF orbit and the OD solution of several SLR orbits in August and September 2018. The CPF orbits are predicted while the OD solution is formed from existing observations. The differences are generally at the 15 m level, although Ajisai is considerably better at about 2 m, and Etalon1 is much worse at about 60 m. The plots are roughly arranged from lowest orbital altitude to highest. The CPF ephemerides were all derived from the Honeywell Technical Services Inc. (HTS) center except Ajisai that was derived from the Japan Aerospace Exploration Agency (JAXA) center.

It appears that the source of the CPF files will change the results. We examined LARES from the NERC Space Geodesy Facility (SGF) instead of HTS and this resulted in the following comparison. Note the improvement from those in Fig. 12.

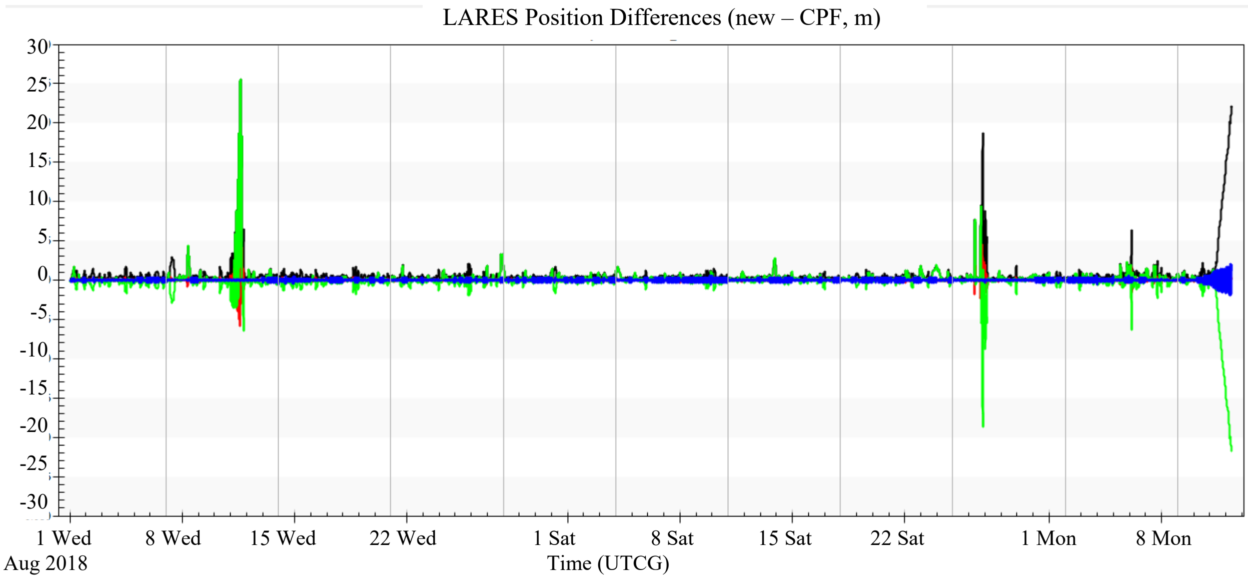

Figure 16: Comparison to CPF orbits: The plots show positional differences between the CPF orbit and the OD solution of LARES in August and September 2018. The CPF orbits are predicted from the SGF center instead of HTS as in Fig. 12. Notice the improvement in the comparison, and the similarity to the results for Ajisai in Fig. 12.

One final check examined the performance of the CPF files to the two-line element (TLE) set files. Admittedly, the TLE solutions have much larger errors, but because the SLR satellites are routinely used for calibration within the AFSPC processing system, they are frequently tracked and have much better orbits than similar objects in the same orbital regimes. It was surprising that there was considerable variability in the accuracy comparisons, and that some lower altitude satellites fared much better than higher satellites. The comparisons were all in the km-level.

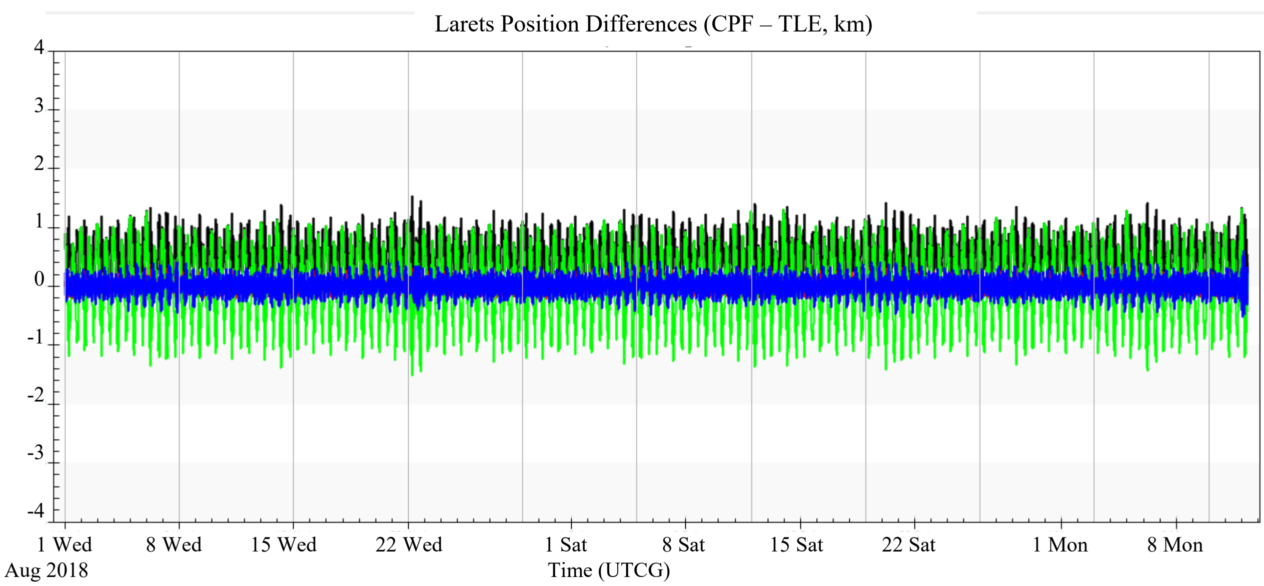

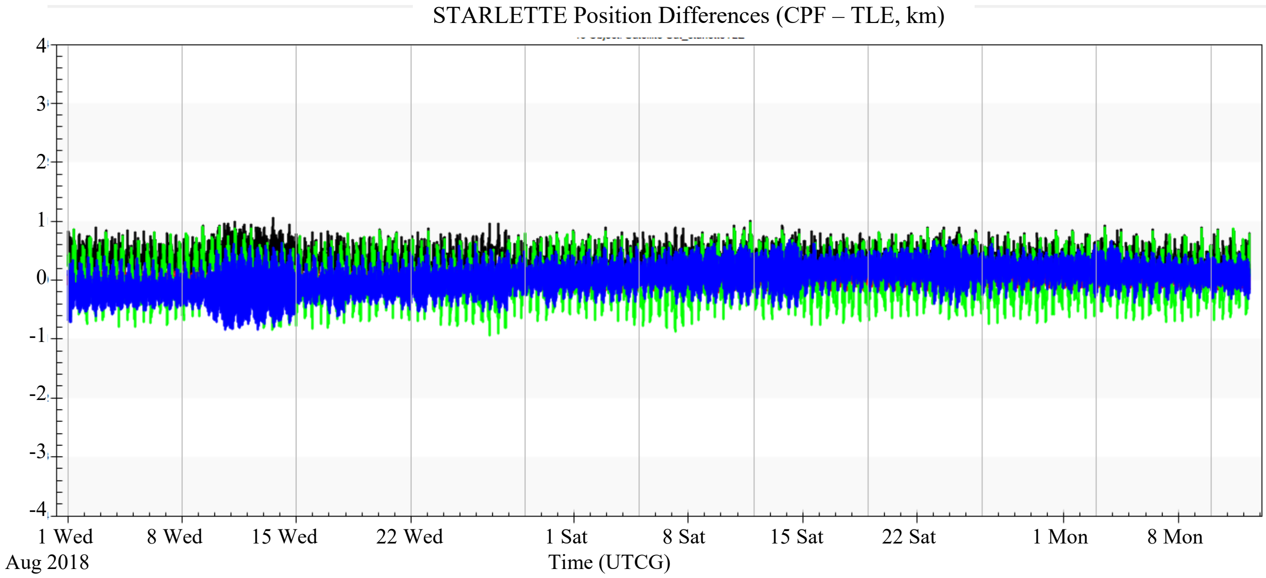
STARLETTE Position Differences (CPF – TLE, km)
4
3
2
1
0
-1
-2
-3
-4
1 Wed
Aug 2018
8 Wed
15 Wed
22 Wed
1 Sat
8 Sat
15 Sat
22 Sat
1 Mon
8 Mon
Time (UTCG)

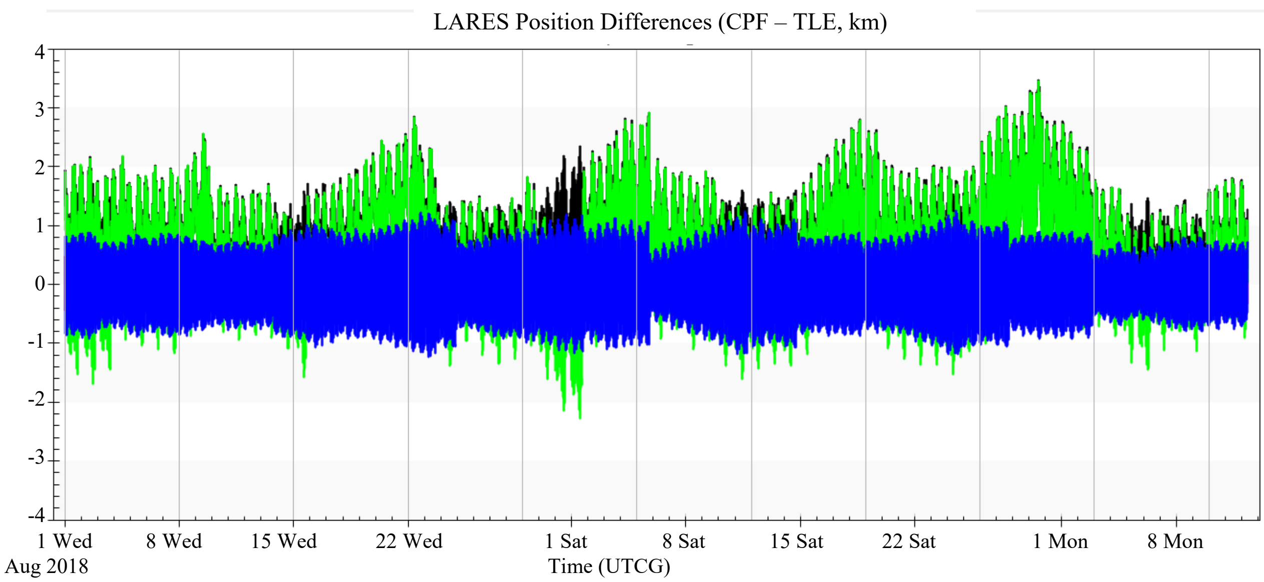
LARES Position Differences (CPF – TLE, km)
4
3
2
1
0
-1
-2
-3
-4
1 Wed
Aug 2018
8 Wed
15 Wed
22 Wed
1 Sat
8 Sat
15 Sat
22 Sat
1 Mon
8 Mon
Time (UTCG)

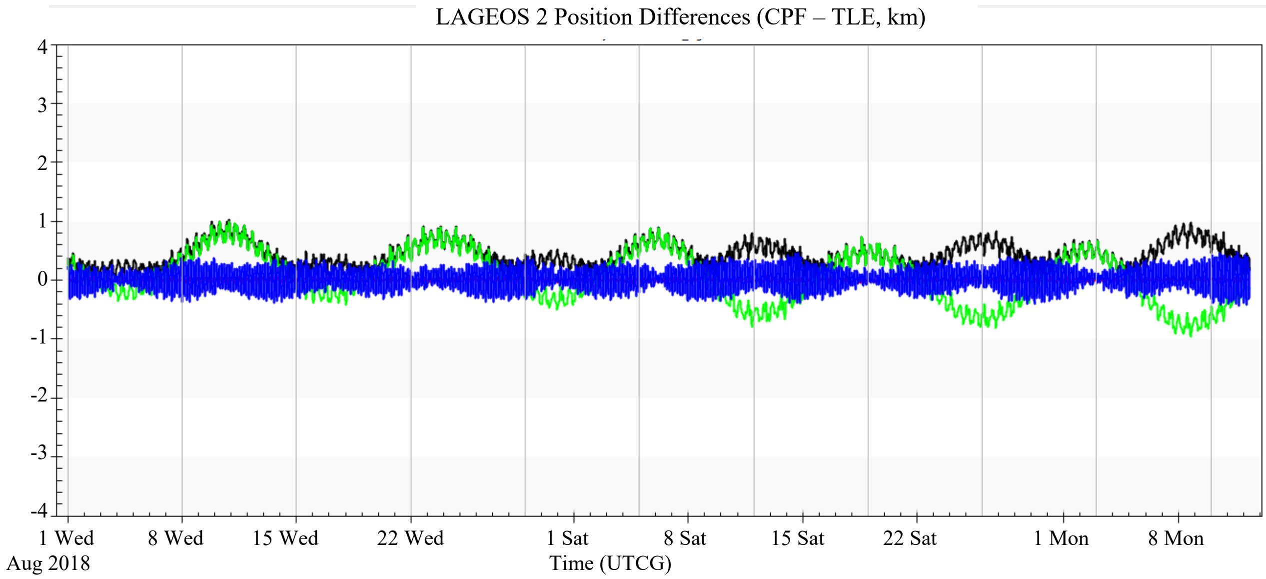

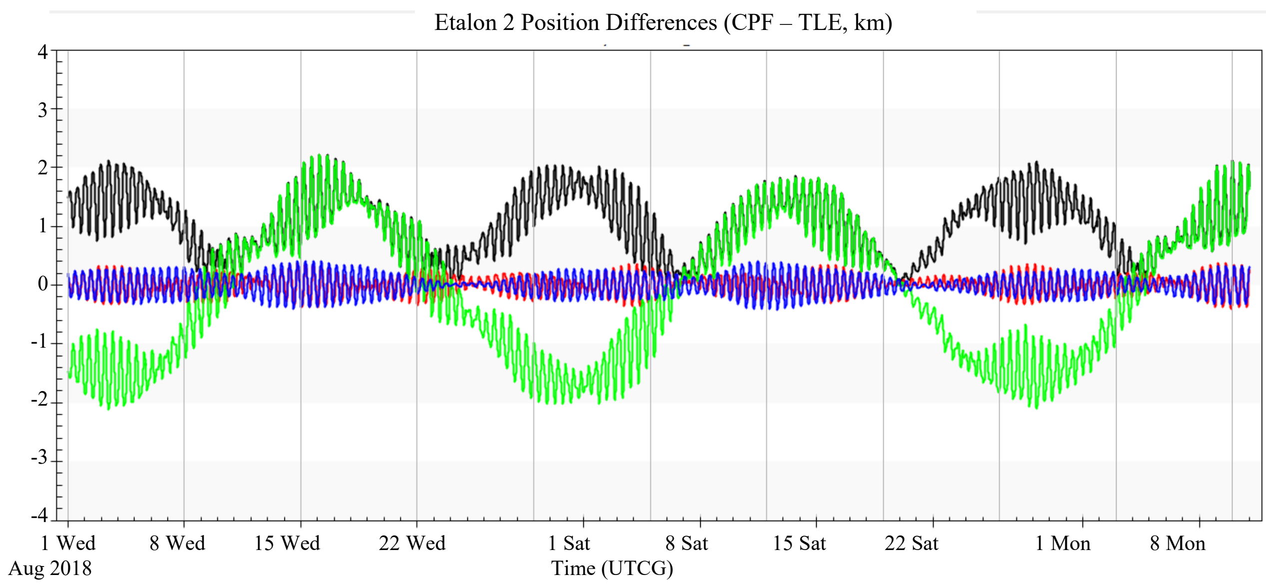

Figure 17: Comparison to CPF orbits: The plots show positional differences between the CPF orbit and the TLE solutions of several SLR orbits in August and September 2018. The CPF orbits are predicted while the TLE solution is formed by AFSPC and their observations from the Space Surveillance Network. The differences are generally at the kilometer level. The plots are roughly arranged from lowest orbital altitude to highest.

CONCLUSIONS

We have processed ILRS data using sequential orbit determination to produce very accurate orbits for calibration efforts with AGI's ComSpOC. Details and sources are specified to configure the ILRS network locations and sensor parameters. Satellite and retro-reflector parameters are listed including sources to update these data. Results of the filter-smoother process are shown, including comparisons to externally generated reference orbits. The overall ability to generate SLR reference orbits has important applications in calibration activities for orbit determination and this paper demonstrates that the new configuration yields similar results to our previous study.

Differences in scenario configuration from that used in our previous study were discussed. Overall, there were not many changes from the prior study, performed 5 years ago. The new configuration includes the latest ITRF-2014 sensor coordinates. We increased the un-modeled cross-track process noise for Etalon 1 and increased the measurement uncertainty for SEJL as the data seemed to indicate greater variability from that sensor.

Several comparisons were made to ensure the accuracy of the new configuration. Comparisons of updated orbit results to those generated with the prior configuration indicated positional differences of generally less than a meter. The predicted ephemerides (CPF) compared well to the updated orbit results as well. Although the CPF ephemerides are not as accurate as an OD solution from observations, the comparisons to the CPF files were just a few meters – which is likely accurate enough for many calibration activities. Note that some of the CPF orbits appeared to have greater variability when compared to the SLR OD solution, and in comparison with the TLE data. It seems that this may be due to the prediction process used by various prediction centers.

At the time of presentation, the LARES solution exhibited greater uncertainty than other satellites we investigated. Subsequent tests revealed process noise values that were a little too large. When corrected, LARES performed comparable to LAGEOS and other SLR satellites. We are appreciative to all the helpful comments received after the presentation.

REFERENCES

Duha, Jânia, Germano B. Afonso and Luiz D. D. Ferreira. 2001. Thermal re-emission effects on the LAGEOS 1 Satellite versus spin axis orientation. *Brazilian Journal of Geophysics*. Vol. 19:2.

Glasserman, Paul. 2004. *Monte Carlo Methods in Financial Engineering*. Springer.

Johnson, Thomas. 2013. Orbit Prediction Accuracy Using Vasicek, Gauss-Markov, and Random Walk Stochastic Models. Paper AAS 13-280 presented at the AAS/AIAA Space Flight Mechanics Conference, February 26-30. Kauai, HI.

Otsubo, T., and G. M. Appleby. 2003. System-dependent center-of-mass correction for spherical geodetic satellites, *Journal of Geophysical Research*. 108(B4), 2201.

Rim, Hyung-Jin. Et al. 2005. ICESat Precision Orbit Determination over Solar Storm Period. Paper AAS 05-138 presented at the AAS/AIAA Space Flight Mechanics Conference, January 23-27. Copper Mountain, CO.

Seago, John H. and Mark A. Davis, and Anne E. Clement. 2000. Precision of a Multi-Satellite Trajectory Database Estimated from Satellite Laser Ranging. Paper AAS 00-180 presented at the AAS/AIAA Space Flight Mechanics Conference, January 23-26. Clearwater, FL.

Uhlenbeck, G. E., and L. S. Ornstein. 1930. On the theory of Brownian motion. Physical Review. Vol. 36:5, pp. 823–841.

Vallado, David A., James Woodburn, and Florent Deleflie. 2014. Sequential Orbit Determination Using Satellite Laser Ranging. Paper AAS 14-287 presented at the AAS/AIAA Space Flight Mechanics Conference, January 26-30. Santa Fe, NM.

Vallado, David A. 2013. *Fundamentals of Astrodynamics and Applications*. Fourth Edition. Microcosm, Hawthorne, CA.

Vallado, David A., et al. 2010. Orbit Determination Using ODTK Version 6. Paper 10A08-1855538 presented at the 4th International Conference on Astrodynamics Tools and Techniques (ICATT) Conference, May 3-6. Madrid, Spain.

Vasicek, Oldrich. 1977. An Equilibrium Characterization of the Term Structure. *Journal of Financial Economics*. Vol. 5 (2): pg 177–188.